Jade1 and the HBO1 complex are spatial-selective cofactors of Oct4

Yifan Wu,[1,2,¶] Asit K. Manna,[1,2,¶] Li Li,[2,3] Hiroshi Handa,[4] Mahesh B. Chandrasekharan,[2,5] Dean Tantin[1,2,*]

[1]Department of Pathology, University of Utah, School of Medicine, Salt Lake City, UT 84112, USA
[2]Huntsman Cancer Institute, University of Utah, School of Medicine, Salt Lake City, UT 84112, USA
[3]Department of Oncological Sciences, University of Utah, Salt Lake City, UT 84112, USA
[4]Center for Future Medical Research, Institute of Medical Science, Tokyo Medical University, Shinjuku, Shinjuku-Ku, Tokyo, 160-8402, Japan
[5]Department of Radiation Oncology, University of Utah, School of Medicine, Salt Lake City, UT 84112, USA

*Correspondence: dean.tantin@path.utah.edu
¶Co-first authors

Running Title: Spatiospecific Oct4 cofactors

Words in Abstract: 239
Manuscript length (including spaces): 66,728
Total Figures: 6
Total Supplemental Figures: 7
Total Supplemental Tables: 3

Abstract

Oct4 is a master regulator of pluripotency. Potential Oct4 interactors have been cataloged extensively but the manner and significance of these interactions are incompletely defined. Like other POU domain proteins, Oct4 is capable of binding to DNA in multiple configurations, however the relationship between these configurations and cofactor recruitment (and hence transcription output) are unknown. Here, we show that Oct4 interacts with common and unique proteins when bound to DNA in different configurations. One of these proteins is Jade1, a component of the HBO histone acetyltransferase complex. Jade1 preferentially associates with Oct4 when bound to More palindromic Octamer-Related Element (MORE) DNA sequences that bind Oct4 dimers and are associated with strong gene expression. Surprisingly, we find that the Oct4 N-terminal activation domain, rather than facilitating Jade1 binding, serves as an autoinhibitory domain that dampens the interaction. ChIP-seq using HBO1, the enzymatic component of the complex, identifies a preference for binding adjacent to Oct4 at MORE sites. Using purified recombinant proteins and nucleosome complexes, we show that the HBO1 complex acetylates histone H3K9 within nucleosomes more efficiently when Oct4 is co-bound to a MORE site. Histone acetylation is further increased when Oct4 is mutated to favor dimeric MORE binding. Cryo-electron microscopy reveals that Oct4 bound to a MORE near the nucleosome entry/exit site partially unwinds DNA from nucleosome core particles, and identifies additional mass associated with the HBO1 complex. These results identify a novel mechanism of transcriptional regulation by Oct4.

Keywords Oct4 (Pou5f1); transcription factors; HBO1/KAT7; Jade1; histone acetyltransferase

50 **Introduction**

51

52 Gene transcription is regulated by the expression and activity of sequence specific DNA binding
53 transcription factors(Stadhouders et al. 2018). Transcription factors differentially regulate different
54 target genes through recruitment of transcription cofactors and action on local chromatin. For
55 example, chromatin modifying enzymes such as histone acetyltransferases (Ogryzko et al. 1996;
56 Wade and Wolffe 1997; Marmorstein and Roth 2001; Utley and Côté 2003) can interact with
57 transcription factors, enhance histone acetylation at local chromatin and favor transcription. Although
58 transcription factor binding specificity in the genome is known to be modulated by interactions with co-
59 expressed transcription factors(Nair et al. 2023), whether the configuration of transcription factor
60 interactions with DNA can influence their interactions with cofactors and hence transcription output is
61 poorly explored.

62 Oct/POU proteins are a group of extended-family homeodomain proteins that play varied roles
63 in development and reprogramming, stress response, somatic stem cell function and the immune
64 response(Tantin 2013; Kim et al. 2021). The canonical monomeric binding site used by class II and
65 class V POU proteins (including Oct4) is the octamer motif, 5'ATGCAAAT(Herr et al. 1988). Variant
66 DNA binding sites have also been described, including two dimeric binding sites known as a PORE
67 (palindromic octamer related element) and a MORE. Structures of the POU proteins Oct1 and Oct4
68 bound to DNA in different configurations, including bound to canonical octamer motifs, MOREs and
69 POREs, have been determined by X-ray crystallography and cryo-electron microscopy (cryoEM)
70 (Klemm et al. 1994; Remenyi et al. 2001; Michael et al. 2020; Sinha et al. 2023a). These studies
71 reveal that while Oct proteins bound to a PORE resemble a dimeric arrangement of two adjacent
72 proteins, binding to a MORE induces a rearrangement of the two DNA binding subdomains (termed
73 POU_S and POU_H) such that both subdomains of the same protein bind to adjacent major grooves on
74 one side the DNA helix, rather than spanning the DNA as in a canonical octamer and a PORE. This
75 unique binding configuration generates unique chemical surfaces of the DNA binding domains and
76 presumably orientations of the N- and C-termini, with the potential to interact with distinct
77 transcriptional regulators. Oct1 and Oct4 binding to genes with MORE sites can be induced by
78 oxidative stress through phosphorylation of the POU_H DNA binding subdomain, which favors
79 intramolecular hydrogen bonding between the DNA binding subdomains to favor MORE binding(Kang
80 et al. 2009). The stabilization can be mimicked with a phospho-mimetic mutation(Kang et al. 2009).
81 This same study also associated MOREs with promoter regions of widely expressed genes such as
82 *Ell*, *Polr2a*, *Rras* and *Rras2*.

83 Here, we identify Jade1 as a selective interactor of Oct4 bound to MORE-containing but not
84 octamer-containing DNA. Jade1 is a component of histone acetyltransferase complexes that contain
85 the MYST family HAT HBO1/KAT7 as the catalytic subunit. Deleting of Oct4 N-terminal activation

86 domain augments the interaction with Jade1. We show that HBO1 and Oct1 are preferentially co-
87 enriched at MORE-containing genes and that Jade1/HBO1 complexes more robustly acetylate H3K9
88 when Oct4 is suppled to nucleosomes containing MORE but not simple octamer DNA near the
89 entry/exit site. An Oct4 mutant with augmented ability to interact with MORE sequences also
90 augments binding to MORE-containing nucleosomes and H3K9 acetylation. ChIPseq experiments
91 with the catalytic HBO1 subunit identify enrichment adjacent to MORE-containing Oct4 target genes.
92 Finally, we use cryoEM to show that Oct4 bound to MOREs near the nucleosome entry/exit site are
93 associated with DNA unwinding, and identify additional densities associated with the HBO1/Jade1L
94 complex. These studies identify Jade1 as a spatioselective cofactor of Oct4.

Results

Oct4 and its cofactors can be enriched by immobilized beads coupled to simple octamer or MORE DNA

To identify interacting proteins with potential selectivity for Oct4 bound to DNA in different configurations, we used magnetic FG beads covalently attached to double-stranded DNA sequences containing multimerized octamer or MORE sequences. In both cases, point mutant DNA was used as a control (Fig. 1A). To reduce the effect of Oct1, an Oct4 paralog co-expressed in ESCs (Shen et al. 2017), we enriched Oct4 from Oct1 deficient ESC extracts. Undifferentiated Oct1-deficient ESCs are hypersensitive to oxidative stress but otherwise normal in terms of gene expression, morphology, and immortality (Shen et al. 2017; Perovanovic et al. 2023). Oct4 bound to wild-type but not mutant DNA sequences (Fig. 1B). The co-enriched materials were then analyzed by ultra-high mass range hybrid quadrupole-orbitrap mass spectrometry (Supplemental Table S1). Comparing material enriched using wild-type vs. mutant octamer DNA (≥2-fold change, $p<0.05$), there were 58 proteins significantly enriched using wild-type DNA, while only 2 proteins were enriched with mutant (Fig. 1C). Proteins enriched using wild-type DNA included Pou5f1 (Oct4), Pou2f3 (Oct11) and Sox2, the latter of which is known to combine with Oct4 at Oct-Sox motifs(Michael et al. 2020). 15 other proteins were previously identified in different reports of Oct4 cofactors (Fig. 1C, black text). Similarly, comparing material enriched using beads coupled to wild-type vs. mutant MORE DNA, there were 27 proteins enriched using wild-type DNA pull-down vs. 6 enriched with point mutant MORE DNA. Proteins enriched using wild-type MORE DNA included once again Pou5f1 (Oct4) and 7 other proteins known to interact with Oct4 (Fig. 1D, black text). These results support the reliability of the mass spectrometry findings.

Comparing the wild-type octamer and MORE enriched proteins, 89.5% (51 out of 57) and 76.9% (20 out of 26) of Oct4 cofactors were specific to either the octamer or MORE sequence DNA. Other than Oct4 itself only six proteins overlap (Supplemental Fig. S1A). This finding is consistent with a hypothesis that different Oct4 configurations preferentially recruit different cofactors. Comparing the enriched proteins with three prior reports on Oct4 interaction partners(Pardo et al. 2010; van den Berg et al. 2010; Ding et al. 2012), we identified 16 overlapping proteins (Supplemental Fig. S1B).

Jade1 associates with Oct4 bound specifically to MORE-containing DNA

One protein strongly co-enriched with Oct4 using beads coupled to wild-type MORE DNA was Jade1, a PHD finger-containing protein thought to act as an adapter subunit of the HBO1 HAT complex that contacts histone H3 and H4 and facilitates its binding to chromatin (Foy et al. 2008; Han et al. 2018; Gaurav et al. 2024). This complex is reported to acetylate histones H3 and H4 with little specificity to activate transcription (Xiao et al. 2021). To test if Jade1 acts as an Oct4 cofactor specifically at MORE

130 sequences, we directly tested Jade1 enrichment using extracts from Oct1 deficient mouse ESCs and
131 FG beads coupled to the four types of DNA sequences (wild-type or mutant octamer or MORE) by
132 Western blotting. Only material enriched using wild-type MORE-coupled beads showed a strong
133 enrichment for Jade1 (Fig. 2A). A replicate experiment confirmed the specificity (Supplemental Fig.
134 S2A). We performed co-immunoprecipitation (co-IP) experiments using antibodies against Oct4 and
135 Jade1, and Oct1 deficient ESC extracts. Both co-IP using Oct4 antibodies and Jade1 Western blot,
136 and reciprocal Jade1 co-IP with Oct4 Western blot identified specific bands (Fig. 2B and C). This
137 interaction was confirmed using extracts from wild-type ESCs (Supplemental Fig. S2B).
138
139 *The Oct4 N-terminus dampens Jade1 recruitment to MORE-containing DNA*
140 Oct4's N-terminus has been shown to harbor an activation domain (Boija et al. 2018). To test if this
141 domain is required for the interaction with Jade1, we deleted the N-terminal 130 amino acids. Prior
142 work has also shown that the Oct4 DNA binding domain contains a nuclear localization sequence
143 (Oka et al. 2013), suggesting that an N-terminally truncated protein retaining the DNA binding domain
144 should still localize to nuclei. We confirmed this prediction using immunofluorescence in 3T3
145 fibroblasts and antibodies against Oct4 (Fig. 2D). We then performed FG bead MORE DNA affinity
146 purification using Expi293F cells transfected with plasmid constructs expressing either full-length or N-
147 terminally deleted Oct4, as well as Jade1. All constructs contained twin-strep tags for efficient
148 detection. N-terminally truncated Oct4 purified from Expi293F cells was selectively degraded during
149 incubation with FG beads, but this could be blocked by including the proteasome MG-132 in the
150 lysates (not shown). This experiment was therefore conducted using 20 μg/mL MG-132 in all lysates.
151 Full-length and N-terminally truncated Oct4 were equivalently expressed (Fig. 2E, lanes 3-4) and
152 associated with MORE-coupled beads equivalently (lanes 7-8). Interestingly, Oct4 lacking its N-
153 terminus more efficiency copurified Jade1 compared to wild-type Oct4 (compare lane 8 to lanes 6 and
154 7). These results indicate that Oct4's N-terminus inhibits the interaction with Jade1.
155
156 *HBO1 preferentially associates near MOREs in ESCs*
157 We attempted to determine Jade1 binding preferences genome-wide using Jade1 ChIP-seq
158 (chromatin immunoprecipitation and sequencing) with an anti-Jade1 antibody without success. We
159 then turned to ChIP using antibodies against the HBO1 subunit of the Jade1/HBO1 complex, HBO1,
160 which has been used successfully in ChIP-seq with HeLa cells (Xiao et al. 2021). Approximately
161 13,800 peaks were identified with high confidence (Supplemental Table S2). HBO1 showed a
162 preference for promoter binding, with 37% of the HBO1 ChIP peaks within ±1 kb of the transcription
163 start site (TSS, Supplemental Fig. S3A), broadly consistent with findings from HeLa cells (Xiao et al.
164 2021). By aligning peaks with TSSs, we found that HBO1 is most highly enriched on either side of the

165 TSS (Supplemental Fig. S3B). We then compared the HBO1 enrichments to Oct4 ChIP-seq data also
166 generated using mouse ESCs(King and Klose 2017). A significant fraction of HBO1 ChIP-seq peaks
167 (1744) overlapped (<200 bp) with Oct4 peaks (Fig. 3A). Studying individual genome tracks, we found
168 that HBO1 ChIP peaks either overlapped with or were immediately adjacent to MORE containing
169 genes such as *Polr2a*, *Zmiz2* and *Rras2*, but were not identified within 2 kb of octamer containing
170 genes such as *Pou5f1* (Fig. 3B). To quantify this more precisely, we calculated the average distance
171 between Oct4 and the nearest HBO1 peak in the total dataset vs. the distance between Oct4 bound at
172 a MORE site and the nearest HBO1. The distance shifted from >10 kb to <200 bp (Supplemental Fig.
173 S3C, Supplemental Table S3).
174 We used MEME-ChIP to directly identify sequences enriched in Oct4 peaks alone compared
175 to overlapping Oct4/HBO1 peaks. Oct4/HBO1 co-enriched targets identified by ChIP-seq preferential
176 enrichment of the MORE over the octamer motif, while Oct4 peaks in isolation, though more
177 abundant, enriched octamer motifs more robustly than MOREs (Fig. 3C). These data indicate that the
178 HBO1/Jade1 complex is recruited by Oct4 more frequently to the MOREs compared to octamer sites.
179
180 *Purified HBO1/Jade1L complexes acetylate histone lysines within nucleosomes*
181 We obtained mammalian expression constructs for recombinant twin-strep-tagged Jade1L (Zhou et al.
182 2002) and purified the protein from Expi293F cells using similar methods as for Oct4. Analysis of the
183 purified Jade1L protein by SDS-PAGE and Coomassie staining revealed the presence of Jade1L at
184 ~100 kDa, as well as several additional bands (Supplemental Fig. S4A), which were identified by
185 Western blotting as HBO-1 (~75 kDa), ING4 (~35 kDa) and hEaf6 (~25 kDa, Supplemental Fig. S4B).
186 Because the purified Jade1L complex contains the HAT enzymatic activity HBO1 and other
187 associated components, we hypothesized that the purified material would acetylate one or more
188 histone lysines within nucleosomes in vitro. The Jade1L/HBO1 complex is known to acetylate histone
189 H4 and the BRPF1/HBO1 complex is known to acetylate histone H3K14(Lalonde et al. 2013; Han et
190 al. 2018). We confirmed that purified Jade1L complex can acetylate histone H4 within nucleosomes
191 (Fig. 4A, lane 2). Blotting with specific antibodies indicates that the purified material can acetylate
192 H4K5, H4K8 and H4K12 but not H4K16 (Fig. 4B, lane 2). Immunoblotting using antibodies specific to
193 H3 acetylation revealed surprisingly no acetylation on H3K14, but robust acetylation at H3K9. H3K18
194 and H3K27 were also not acetylated by purified Jade1L/HBO1 complex (Fig. 4B, lane 2).
195
196 *Oct4 bound to a MORE augments histone H3K9 acetylation by Jade1L/HBO1*
197 We tested the effect of Oct4 bound to MORE DNA on Jade1L/HBO1-mediated in vitro HAT activity
198 using purified nucleosomes as a substrate. Surprisingly, acetylation at all histone H4 lysines was
199 reduced to different extents upon inclusion of purified Oct4, whereas the acetylation on lysine 9 on
200 histone H3 was increased (Fig. 4B, lane 3). To test if there is any effect on Oct4 binding stoichiometry

201 in presence of Jade1L, we tested Oct4 binding to MORE containing DNA in the presence and
202 absence of Jade1L. Interestingly the extent of the dimeric form of Oct4 bound to DNA increased in
203 presence of Jade1L (Fig. 5A). Oct1 can also bind to MOREs(Remenyi et al. 2001), and point mutation
204 of Oct1 at S385D on a loop region of POU_H that allows for intramolecular hydrogen bonding with
205 POU_S to stabilize the MORE-bound configuration increases the dimeric compared to monomeric
206 form(Kang et al. 2009). Because this region is highly conserved between Oct1 and Oct4, we were
207 able to generate the analogous mutation in the Oct4 DNA binding domain, $Oct4^{S229D}$, in the context of
208 the Oct4 expression construct (Supplemental Fig. S4C). As expected, $Oct4^{S229D}$ bound more
209 efficiently to the MORE compared to Oct4. Interestingly the $Oct4^{S229D}$ protein that bound more strongly
210 to MOREs also augmented H3K9 acetylation by the Jade1L/complex compared to wild-type Oct4 (Fig.
211 5C).
212
213 *CryoEM structure of the HBO1/Jade1/ING4/hEaf6 complex and $Oct4^{S229D}$ in the presence of a*
214 *nucleosome*
215 We reconstituted the HBO1/Jade1/ING4/hEaf6 nucleosome complex in the presence of $Oct4^{S229D}$
216 using purified recombinant proteins (Supplemental Fig. S5-B) incubated at equimolar ratios for 30 min
217 over ice. We processed 6200 dose-fractionated cryoEM images (Fig. 6B and Supplemental Fig. S6A)
218 to elucidate the structure of the complex. The best reconstructed and refined 3D volume with 7.2 Å
219 resolution and a B Factor 322 (Fig. 6D and Supplemental Fig. S6A, center) showed an extension of
220 DNA and extra volume surrounding the nucleosome core resulting in a more spherical structure (Fig.
221 6D), consistent with a nucleosome/HAT complex. The structural resolution was insufficient to model
222 the position of HBO1, Jade1, ING4 or hEaf6, however the dimeric Oct4 POU_S and POU_H domains
223 (PDB ID: 7XRC) could be manually fitted into the extended volume (Fig. 6E, left and right). A
224 nucleosome core structure (PDB ID: 6TEM) could also be fitted into the 3D volume, with the 5' part of
225 the DNA sequence removed and replaced with linear B-form DNA to complete the volume (Fig. 6F left
226 and right). This result is consistent with an interpretation in which dimeric Oct4 bound near the
227 nucleosome entry/exit site in the presence of the HBO1 HAT complex partially unwinds DNA from
228 core nucleosomes.

229 **Discussion**

230

231 The ability of transcription factors bound to DNA in different configurations to interact with distinct
232 cofactors is incompletely understood. Nevertheless, different specificities can be predicted because
233 proteins associated with DNA in different configurations necessarily present different chemical
234 docking surfaces. For example, the Oct4 paralog Oct1 can associate with its B and T cell-specific
235 coactivator OCA-B (OBF-1, Bob.1) when bound to a simple octamer or a PORE but not when bound
236 to a MORE due to occlusion of the docking site in the MORE configuration (Tomilin et al. 2000). It has
237 been speculated that perhaps there are many such examples with POU proteins which can rearrange
238 their DNA binding domains based on the orientation and spacing of their cognate DNA half-sites
239 (Pesce and Schöler 2001). As a second example, FoxP3 binds to DNA as a dimer in a head-to-head
240 conformation, forming a hydrophobic pocket for Runx1 binding in normal regulatory T cells and
241 leading to immune tolerance. However, some human immunodysregulation polyendocrinopathy
242 enteropathy X-linked (IPEX) patients harbor a *FOXP3* mutation that encodes a protein that binds to
243 DNA in a "forkhead-swapped" configuration in which the DNA binding domains bind DNA in a different
244 configuration resulting in no Runx1 binding pocket(Bekere and de Oliveira Mann 2022). Here, we
245 show that the pluripotency master regulator Oct4, bound to DNA in different monomeric and dimeric
246 configurations, selectively associates with distinct cofactors. One of these, the Jade1 component of
247 the HBO1 complex, associates with Oct4 bound as a homodimer bound to DNA sites known as
248 MOREs (Fig. 7).

249 Prior studies have investigated potential Oct4 and other interactions partners(Pardo et al.
250 2010; van den Berg et al. 2010; Ding et al. 2012), however, these studies did not specifically analyze
251 interactions with DNA-bound Oct4. Moreover, within the genome, Oct4 sites are known to be
252 complex, frequently comprising different octamer half-sites with variable numbers, spacing and
253 orientation (Tantin et al. 2008; Ferraris et al. 2011) and frequently closely associated with binding
254 sites for other transcription factors. For example, in pluripotent stem cells a single molecule of Oct4
255 binds to an Oct:Sox element approximately 2 kb upstream of the *Pou5f1* gene as a heterodimer with
256 Sox2(Chew et al. 2005), while four Oct4 molecules are capable of binding upstream of *Polr2a* at two
257 consecutive MOREs(Kang et al. 2009). We used canonical octamer element or MORE DNA to enrich
258 Oct4 and co-bound proteins from mouse embryonic stem cell extracts. We opted to use ESCs
259 deficient in the Oct4 paralog Oct4 rather than wild-type ESCs (Shen et al. 2017; Perovanovic et al.
260 2023) to avoid confounding unique proteins bound by this protein, though we validated the findings
261 using wild-type ESCs. Analyzing the bound proteins using mass spectroscopy, we identified several
262 proteins consistent with prior reports, including Sox2 and Mta1(Pardo et al. 2010; van den Berg et al.
263 2010). Proteins associated with Oct4 bound to canonical octamer sites tended to be associated with
264 transcriptional repression, e.g. Macroh2a1 (Campos and Reinberg 2009; Martire and Banaszynski

265 2020), Ctbp2 (Chinnadurai 2009), Mta1 (Liang et al. 2008), Kdm2b (Isshiki and Iwama 2018). In
266 contrast, many MORE-associated proteins are associated with transcription activation, e.g. H3.3
267 (Campos and Reinberg 2009; Martire and Banaszynski 2020) and Jade1 itself. This may reflect that
268 fact that Oct4 operating through canonical octamer DNA has been associated with both activation and
269 repression (Ambrosetti et al. 1997; Liang et al. 2008), while MORE-containing genes such as *Polr2a*,
270 *Ahcy*, *Rras*, *Ell* and *Taf12* tend to be broadly and strongly expressed. Reporter assays have shown
271 that dimeric Oct4 activates gene expression far more strongly than monomeric Oct4 (Botquin et al.
272 1998).

273 Proteins specifically enriched using MORE-containing DNA included Jade1, a PHD finger-
274 containing scaffolding protein that recognizes histone H3 and helps localize HBO1-contaning HAT
275 complexes to chromatin(Gaurav et al. 2024). In human ESCs, HBO1 deficiency is associated with
276 loss of pluripotency and spontaneous neural differentiation, and a defect in mesendoderm
277 specification following TGFβ treatment(Zhang et al. 2024). We confirmed the Oct4-Jade1 interaction
278 using co-IP. Because the Oct4 N-terminus has been associated with activation (Boija et al. 2018), we
279 tested whether the N-terminus was important for this interaction. Oct4 contains a nuclear localization
280 sequence in its homeodomain (Oka et al. 2013), preserving nuclear localization in the N-terminally
281 truncated Oct4 construct. Surprisingly, Oct4 lacking its N-terminus showed superior interactions with
282 Jade1. We propose that Oct4 binding to a MORE orients Oct4 molecules to relieve occlusion of Jade1
283 by the Oct4 N-termini, whereas Oct4 binding to a canonical site allows for the recruitment of other
284 coregulators, via the N-terminus, to regulate gene expression at pluripotency-associated targets,
285 developmentally poised targets, and other targets lacking MOREs (Supplemental Fig. S7). The Oct4
286 N-terminus is a site of post-translational modification (Nishi et al. 2011; Brumbaugh et al. 2012),
287 potentially adding another layer of regulation.

288 HBO1 ChIP-seq studies using Oct1 deficient mouse ESCs identify ~12,000 binding events and
289 reveal a preference for promoter binding, similar to findings using HBO1 ChIP-seq in HeLa cells (Xiao
290 et al. 2021). Intersecting these peaks with known Oct4 binding sites identifies ~1,700 co-binding
291 events preferentially enriched for MOREs, which are otherwise rare in the genome compared to
292 canonical octamer elements. In ESCs, HBO1 preferentially associates with DNA adjacent to MOREs
293 at target genes.

294 Purified recombinant Oct4 bound to MOREs adjacent to nucleosomes catalyzes increased
295 acetylation of H3K9 but not other lysines by HBO1/Jade1 complexes in a reconstituted system.
296 Lysines in H4 for example were efficiently acetylated by reconstituted HBO1/Jade1-containing
297 complexes, however only histone H3K9 showed an augmentation in acetylation in the presence of
298 Oct4 and MORE DNA. Moreover, we showed that conditions that augment Oct4 binding also augment
299 H3K9 acetylation. Prior work showed that Oct4 can regulate transcription through H3K9 methylation

300 via the recruitment of Jmjd1c (Shakya et al. 2015b). Prior work showed that MORE binding by the
301 Oct4 paralog Oct1 is inducible through a specific serine residue that when phosphorylated stabilizes a
302 MORE-bound DNA binding configuration, and that a phospho-mimetic mutation augments MORE
303 binding(Kang et al. 2009). We found that the analogous mutation in Oct4 (Oct4^{S229D}) also
304 preferentially bound to MORE DNA. The increase in Oct4 binding was associated with increased
305 HBO1-mediated H3K9 acetylation. The lack of augmentation of H4 acetylation is surprising, however
306 the Oct4 N-terminus is known to bind to the H4 tail (Sinha et al. 2023b) and may occlude additional
307 acetylation via this mechanism. Oct4 is known to recruit cofactors that act on H3K9 by removing
308 K9me2 marks (Shakya et al. 2015a).
309 Using the same recombinant proteins used in the HAT assay, we also determined the cryoEM
310 structure of the complete complex at ~7 Ä resolution, revealing that the complex surrounds both sides
311 of the nucleosome to form a more spherical structure, and revealing that the DNA partially unwinds
312 from the nucleosome core to generate an extension containing the MORE and Oct4 homodimer.
313 Oct4 binding to DNA, particularly through multiple binding sites, is known to induce changes in
314 nucleosome structure, including repositioning of DNA and altering the location of the H3 and H4 tails
315 (Sinha et al. 2023b). Cumulatively, these results highlight Oct4 as a prime example of a
316 spatioselective transcription factor that can interact with difference coregulatory proteins when bound
317 to DNA in different configurations.
318

Materials and Methods

Cell culture

Embryonic stem cells (ESCs) were cultured on mitomycin C-arrested feeder MEFs in ES medium as described in (Shakya et al. 2015b) in the presence supplemented LIF and 2i conditions (3 μM CHIR99021 and 1 μM PD0325901, Selleck Chemicals) at 37°C. One passage prior to experiments, the feeders were depleted by culturing on gelatin coated plates overnight. 293T cells were cultured with DMEM medium with 10% FBS and 1x GlutaMAX supplement (ThermoFisher). Expi293F cells were grown in Expi293 expression media (ThermoFisher #A1435101) in shaker flasks at 37°C in a humidified incubator supplied with 8% CO_2 equipped with a shaker set to125 rpm. For transfection, Expi293F cells were seeded in 30 mL of Expi293 expression media at a density of 1.25×10^6 cells/mL in 125 mL flasks. After 24 hr, cells were transfected with wild-type Oct4 expression plasmids (Shen et al. 2024), $Oct4S^{229D}$ mutant plasmids or Jade1L (Zhou et al. 2002) using an ExpiFectamine 293 Transfection Kit (ThermoFisher) following the manufacturer's protocol.

Immobilization of dsDNA on FG beads

Double-stranded DNA (dsDNA) was covalently fixed to FG magnetic beads (Tamagawa-Seiki) using the manufacturer protocol. Briefly, 150 μg of sense and antisense 5' phosphorylated single-stranded DNA (WT octamer sense: 5'-ACGTATGCAAATAGTGGGGG-3', WT octamer antisense: 5'-ACTATTTGCATACGTCCCCC-3'; mutant octamer sense: 5'-ACGTA<u>AA</u>C<u>T</u>A<u>C</u>TAGTGGGGG-3', mutant octamer antisense: 5'-ACTAGTAGTTTACGTCCCCC-3'; WT MORE sense: 5'-CATGCATATGCATGCGGGGG-3', WT MORE antisense: 5'-GCATGCATATCGATGCCCCC-3'; and mutant MORE sense: 5'-CACACTGTCGTGTGCGGGGG-3', mutant MORE antisense: 5'-GCACACGACAGTGTGCCCCC-3' where underlined text indicates the mutation) dissolved in ultrapure water at 1 μg/μL were annealed at 98°C for 10 min and gradually cooled to the room temperature. The annealed dsDNAs were ligated using 700 units of T4 DNA ligase (New England Biolabs) on a rocker platform at 37°C overnight. Ligated DNA was size-selected using a NICK column (GE Healthcare, 200bp-400bp) and eluted in 400 mL ultrapure water. 400 μL DNA (approximately 250 μg/mL) were immobilized to 10 mg of ultrapure water-washed FG beads at 50°C for 24 hr. The beads were then washed with 2.5 M KCl twice, ultrapure water twice and TES buffer (10 mM Tris-HCl pH 8.0, 0.3 M KCl, 1 mM EDTA and 0.02% NaN_3) three times. Immobilized beads were dispersed in 400 mL of TES buffer and stored at 4°C. Beads contained at least 2 μg immobilized DNA per mg.

Oct4 affinity purification

353 ESCs deficient for the transcription factor Oct1 (Shen et al. 2017; Perovanovic et al. 2023) were
354 pelleted and resuspended in NP-40 lysis buffer (150 mM NaCl, 1% NP-40, 50 mM Tris-Cl pH 8.0)
355 containing cOmplete protease inhibitor cocktail (Roche) and PhosSTOP phosphatase inhibitor cocktail
356 (Roche). Cells were lysed by rotating in the buffer and clarified by centrifugation at 13,000×*g* at 4°C.
357 Protein concentrations were normalized using Bradford assays (Bio-Rad) and diluted (>5-fold) to 1
358 mg/mL using 100 mM KCl buffer (100 mM KCl, 10% glycerol (v/v), 20 mM HEPES pH 7.9, 2 mM
359 $MgCl_2$, 0.2 mM $CaCl_2$, 0.2 mM EDTA, 0.1% NP-40, 1 mM dithiothreitol) with protease and
360 phosphatase inhibitors. DNA-immobilized FG beads were washed with 100 mM KCl buffer, and 0.5
361 mg of the beads were added to the diluted cell lysates and rotated at 4°C for 4 hr. The beads were
362 sequentially washed 3 times with 100, 200 and 300 mM KCl buffer. Bound proteins were eluted with
363 300 mM KCl buffer containing 30 μM of the corresponding free DNA oligomers for 1 hr at 4°C on a
364 rotating platform. For experiments testing Oct4 lacking its N-terminus, lysates contained 20 μg/mL
365 MG-132 (Sigma) and post-binding to MORE DNA-conjugated FG beads were washed three times
366 with 100 mM KCl buffer.
367
368 *Western blotting*
369 Jade1L, HBO1, ING4 and hEaf6 proteins were detected using antibodies from Novus (NBP1-83085),
370 Abcam (ab124993), Abcam (ab108621) and Novus (NBP1-91523) respectively. Recombinant Oct4
371 and Oct4 S229D were detected using an antibody from Santa Cruz (sc-5279). Twin-strep-tagged
372 proteins were detected using HRP conjugated anti-StrepII antibody (Genscript). Acetylated Histone
373 H4 was detected by Abcam H4 antibody cat no ab177790. Histone H3 was detected using an
374 antibody from Cell Signaling Technology (CST, 4499T). H4K5, H4K8, H4K12, H4K16, H3K9, K3K14,
375 H3K18 and H3K27 acetylation were detected using monoclonal antibodies from CST (8647T, 2594T,
376 13944T, 13534, 96495, 7627T, 13998T and 8173T respectively).
377
378 *Mass spectrometry and analysis*
379 Proteins eluted from DNA-bound FG beads above were resolved by 10% SDS-PAGE approximately 2
380 cm unto the running gel and stained with Colloidal Blue (Invitrogen). The gel slabs were excised and
381 destained until they were clear. Proteins in the gel slabs were reduced with 25 mM DTT at 37°C for 30
382 min, followed by alkylation with 50 mM IAA for 45 min at room temperature. Proteins were then
383 digested with 1.0 μg of trypsin overnight at 37°C. The peptides were extracted from the gel, dried
384 completely, desalted and suspended in 20 μL of 0.1% formic acid for LC-MS/MS analysis. Reverse-
385 phase nano-LC/MS/MS was performed on an UltiMate 3000 RSLCnano system (Dionex) coupled to a
386 ThermoScientific Q Exactive-HF mass spectrometer equipped with a nanoelectrospray source.
387 Peptides were diluted to 0.2 μg of sample in 0.1% formic acid in water. 5 μL of the samples were

388 injected onto the liquid chromatograph. A 50-cm long/100 μm inner diameter reverse-phase BEH C18
389 3.0 μm nanocolumn (ThermoFisher) was employed for chromatographic separation. A gradient of
390 buffers (Buffer A: 0.1 % formic acid in water; Buffer B: 0.1% formic acid in acetonitrile) at a flow rate of
391 200 μL/min at 60°C was used. The LC run lasted for 83 min with a starting concentration of 5% buffer
392 B increasing to 55% over the initial 53 min and a further increase in concentration to 95% over 63 min.
393 MS/MS data was acquired using an auto-MS/MS method selecting the 20 most abundant precursor
394 ions for fragmentation. The mass-to-charge range was set to 350–1800. For these samples, the
395 Uniprot database was searched with the *Mus musculus* taxonomy selected. An allowance was made
396 for 2 missed cleavages following trypsin/Lys-C digestion. The fixed modification was cysteine
397 carbamidomethylation. The variable modifications were methionine oxidation, and N-terminal
398 deamidation. The search was performed with a mass tolerance of 15 ppm for precursor ions and a
399 mass tolerance of 10 ppm for fragment ions. Protein enrichment was analyzed by MASCOT using
400 N=3 biological replicates. The raw data were processed by MetaboAnalyst(Pang et al. 2021), and the
401 missing values were estimated by KNN. Raw data were processed with log transformation and Pareto
402 scaling. The threshold was set as 2-fold enrichment and $p<0.05$.
403
404 *Oct4 N-terminal deletion*
405 Oct4 fused with C-terminal twin-strep and FLAG tags cloned into the pACE-MAM2 vector (Geneva
406 Biotech) for mammalian cell expression was described previously (Shen et al. 2024). The N-terminal
407 Oct4 truncation lacking the first 130 amino acids was generated by PCR amplification with primers 5'-
408 ctcaatcCATGGACATGAAAGCCCTGCAG-3' and 5'-GAATGCATCAGCTGGTTTGAATGCATGGG-3'
409 where the lower-case letters indicate divergence from the parent vector. The wild-type and N-terminal-
410 truncated Oct4 PCR fragments were digested with *Nco*I and *Pvu*II and ligated back into the pACE-
411 MAM2 vector digested with *Nco*I and *Pvu*II to generate the truncated Oct4 vector. All constructs were
412 sequenced to confirm veracity.
413
414 *Co-IP*
415 ESCs and 3T3 cells transfected with the Oct4 or Oct4ΔN plasmids described above were lysed with
416 RIPA buffer (150mM NaCl, 50mM Tris-HCl pH 8.0, 1% NP-40, 0.5% sodium deoxycholate, 0.1%
417 SDS) containing cOmplete protease inhibitor cocktail (Roche) by rotating at 4°C for 30 min. Lysates
418 were clarified by centrifugation (13,000xg) for 10 min. 2 μg of primary antibodies were added to the
419 lysates, which were rotated at 4°C overnight. Antibodies used were as follows: anti-Oct4 (Santa Cruz
420 sc-5279), anti-Jade1 (Proteintech 15032-1-AP), anti-FLAG M2 (Sigma-Aldrich F1084). Isotype control
421 IgG was purchased from Jackson ImmunoResearch. 20 μL RIPA buffer-washed Protein G Dynabeads
422 (ThermoFisher 10004D) were added to the cell lysis-antibody mix, which were rotated at 4°C for an
423 additional 5 hr. Protein-bound Dynabeads were then washed with 500 μl RIPA buffer for 4 times, and

424 proteins were eluted with 50 µL 2x SDS loading buffer (4% SDS, 20% glycerol, 0.2% bromophenol
425 blue, and 200 mM DTT) by heating at 98°C for 5 min.
426
427 *ChIP-seq*
428 ChIP-seq was performed as previously described (Perovanovic, Wu et al. 2023). Briefly, Oct1
429 deficient ESCs were crosslinked with 1% formaldehyde, quenched with 2.5 M glycine, and crude
430 nuclei were extracted using Farnham lysis buffer (5 mM PIPES pH 8.0, 85 mM KCl, 0.5% NP-40), and
431 further lysed with RIPA lysis buffer. Chromatin was sheared on ice using EpiShear probe sonicator
432 (Active Motif) set to amplitude=40, 30 sec on/30 sec off for 5 min. 4 µg of rabbit anti-HBO1 antibody
433 (Cell Signaling #58418S) was applied to the sheared chromatin and the mixture incubated at 4°C
434 overnight. 1.5 mg of protein G Dynabeads (ThermoFisher) were applied to samples, which were
435 rotated at 4°C for 5-6 hr to allow binding, and the beads were collected and washed with Low Salt
436 buffer (20 mM Tris-Cl pH 8.0, 150 mM NaCl, 2 mM EDTA, 0.1% SDS, 1% Triton X-100), High Salt
437 buffer (identical but with 500 mM NaCl), Low Salt buffer, LiCl buffer, and TE buffer (Tris-EDTA pH 8.0
438 plus 1 mM EDTA) for 5 washes in total, each with 10 min rotating at 4°C. Chromatin was eluted from
439 the beads using IP Elution buffer (1% SDS and 0.1M $NaHCO_3$) and incubated at 65°C overnight to
440 reverse the formaldehyde crosslinks. Before IP, 2% Input was reserved from the samples. DNA was
441 purified from both IP samples and input using phenol-chloroform-isoamyl alcohol extraction followed
442 by QIAquick PCR purification kit (Qiagen). N=2 biological repeats were performed per condition. ChIP
443 materials were sequenced using a NovaSeq instrument (Illumina).
444
445 *ChIP-seq analysis*
446 Between 16 and 25 million paired-end reads were aligned to the mouse Mm10 reference genome
447 using Novoalign v4.03.01. HBO1 and Oct4 ChIP-seq data was analyzed using Macs2 (Zhang, Liu et
448 al. 2008), with parameters of q 0.005, max-gap 100 and q 0.005, max-gap 100, min-length 200
449 respectively. HBO1 and Oct4 ChIP peak summits within 100 bp were defined as overlapping peaks.
450 Oct4 peaks and overlapping peaks were analyzed with MEME-chip CentriMo (Bailey and Machanick
451 2012) for motif enrichment. The raw and processed ChIP-seq data have been deposited with the gene
452 expression omnibus (GEO, series record GSE279191).
453
454 *Recombinant Oct4 and Jade1 purification*
455 Wild-type Oct4 expression plasmids (Shen et al. 2024) were transfected into Expi293F cells
456 (ThermoFisher) using the ExpiFectamine 293 Transfection Kit (ThermoFisher) following the
457 manufacturer instructions. 48 hr post-transfection, cells were harvested and washed with ice-cold
458 PBS. Cells were resuspended in Buffer A (20 mM HEPES pH 8.0, 1.5 mM $MgCl_2$, 10 mM KCl, 0.25%
459 NP-40, 0.5 mM dithiothreitol) containing protease inhibitor cocktail (Roche), incubated for 10 min on

460 ice, and homogenized using a Dounce homogenizer (Wheaton). The homogenate was centrifuged at
461 4°C for 5 min at 3800×*g* to pellet nuclei, which were resuspended in Buffer C (20 mM HEPES pH 8.0,
462 25% glycerol, 1.5 mM MgCl2, 420 mM KCl, 0.25% NP-40, 0.2 mM EDTA, 0.5 mM dithiothreitol) with
463 protease inhibitors and again Dounce homogenized. Nuclei were extracted for 30 min at 4°C with end-
464 to-end rotation, then centrifuged at 4°C for 30 min at 20,000×*g*. The nuclear extract was then
465 immunoprecipitated with anti-FLAG (M2)-agarose beads (Sigma). Bead-bound proteins were eluted
466 with 200 ng/µL 3´FLAG peptide (Sigma) by incubating at 4°C for 30 min. To generate an Oct4 point
467 mutation corresponding to Oct1 S385D (Kang et al. 2009), Oct4 S229 was mutated by overlap
468 extension PCR using as middle primers 5'-GAGAAAGCGAACTGATATTGAGAACCG-3', 5'-
469 CGGTTCTCAATATCAGTTCGCTTTCTC-3', and as end primers 5'-GGATCTCGAGCCATGGCTGG-
470 3', 5'-GAATTAGGTACCTTATTTGTCATCATCG-3'. For Jade1 purification, 60 µg of full-length Jade1
471 expression plasmid (Zhou et al. 2002) (a gift from Dr. Jacques Côté) was used and purified similarly.
472 All proteins were pure and monodisperse as verified using SDS-PAGE/Coomassie blue staining and
473 size exclusion chromatography.
474
475 *Baculovirus expression for cryoEM*
476 The pFastBac-1 vector was digested with *BamHI* and *EcoRI* and ligated with annealed oligos 5'-
477 GATCCATGTCGCATCACCATCACCATCACAGGCTCGAGGCCATGGTG-3' and 5'-
478 AATTCACCATGGCCTCGAGCCTGTGATGGTGATGGTGATGCGACATG-3' to incorporate a 6-His
479 tag as well as *Xho*I and *Nco*1 sites. A single base frameshifted version of pFastBac-1 was also
480 generated using the oligos 5'-
481 GATCCATGTCGCATCACCATCACCATCACGAGGCTCGAGGCCATGGTG-3' and 5'-
482 AATTCACCATGGCCTCGAGCCTCGTGATGGTGATGGTGATGCGACATG-3'. cDNAs encoding wild-
483 type or S229D Oct4 with C-terminal twin-strep and FLAG-tags were then subcloned into the modified
484 pFastBac-1 vector between the *Nco*I and *Kpn*I sites. The *Ing4* cDNA was amplified using PCR from a
485 plasmid template (Addgene #13289) using 5'-AGGCTCGAGATGGCTGCGGGGATG-3' and 5'-
486 AGAATGCATTTTCTTCTTCCGTTCTTGG-3' primers and was cloned into the *Xho*I and *Nsi*I sites
487 using the Oct4/pFastBac-1 vector by first excising the Oct4 cDNA using *Xho*I and *Nsi*I, preserving the
488 N-terminal His-tag and C-terminal twin-strep tags. HBO1 and hEaf6 gene blocks containing C-terminal
489 twin-strep-tag were synthesized from IDT and cloned into the modified single-base frameshifted
490 pFastBac1 vector using the *Xho*I and *Kpn*I sites. Full-length Jade1L was cloned in the backbone of
491 the Oct4 expression plasmids (Shen et al. 2024) using the *Xho*I and *Nsi*I sites to replace Oct4, then
492 Jade1L with a C-terminal twin-strep tag was amplified by PCR from the Jade1L mammalian cell
493 expression plasmid using the primers sets 5'-GATCTCGAGCCATGAAACGAGGTCGCCTTCC-3' and
494 5'-TATGCATGCTTATTTGTCATCATCG-3' and cloned into the *Xho*I and *SphI* sites of the modified

495 single-base frameshifted pFastBac-1 vector. Constructs were transposed into bacmids using
496 DH10Bac competent cells (ThermoFisher #10361012). Transposed recombinant bacmids were
497 purified using a PureLink plasmid isolation kit (ThermoFisher #K210004). Transposition was
498 confirmed by PCR. Recombinant bacmids were transfected into Sf9 cells to generate recombinant
499 virus and amplified for large scale protein purification by growth to 3-4$\times10^6$ cells/mL in Sf-900 II SFM
500 media (ThermoFisher #10902088) in a humidified 28°C incubator shaking at 125 rpm. Cells were
501 collected, added to fresh media at 2$\times10^6$ cells/mL, and infected with recombinant baculovirus. Cells
502 were grown for 48 hr, harvested by centrifugation and lysed in lysis buffer (20 mM HEPES pH 8.0,
503 300 mM NaCl, 5% glycerol, 0.5mM DTT) containing protease inhibitor cocktail (Roche) using an
504 Active Motif probe sonicator. The lysate was centrifuged at 22700$\times$*g* for 30 min. The supernatant was
505 loaded onto a 1 mL prepacked Strep-tactin XT column (Cytiva #29401317), washed with 10 column
506 volumes of wash buffer (20 mM HEPES pH 8.0, 300 mM NaCl, 5% glycerol, 0.5 mM DTT), and eluted
507 with wash buffer containing 50 mM biotin (Sigma). Purity was confirmed by 12% SDS-PAGE and
508 Coomassie staining.
509
510 *Nucleosome preparation*
511 153 bp DNA constructs containing either MORE
512 (ATCCTGGAGAAATGCATATGCATGGCCGCTCAATTGGTCGTAGACAGCTCTAGCACCGCTTAAA
513 CGCACGTACGCGCTGTCCCCCGCGTTTTAACCGCCAAGGGGATTACTCCCTAGTCTCCAGGCAC
514 GTGTCAGATATATACATCCTGTGAT) or octamer sequence
515 (ATCCTGGAGAATCCCGGATGCAAATCCGCTCAATTGGTCGTAGACAGCTCTAGCACCGCTTAAA
516 CGCACGTACGCGCTGTCCCCCGCGTTTTAACCGCCAAGGGGATTACTCCCTAGTCTCCAGGCAC
517 GTGTCAGATATATACATCCTGTGAT) were designed based on the octamer binding site as
518 previously described (Michael et al. 2020). 16 copies of the DNA were cloned into the pUC19 vector
519 using published methods(Wu et al. 2016). The plasmid containing 16 copy of desired DNA fragment
520 was prepared by large scale plasmid purification followed by *Eco*RV-HF digestion. The final fragment
521 was purified by PEG8000 precipitation(Lis and Schleif 1975). Recombinant human histones H2A,
522 H2B, H3.3 and H4 were expressed from transfected plasmids (Ye et al. 2019) (a gift from Dr. Brad
523 Cairns) and individually purified from Rosetta2 DE3 cells (Sigma-Aldrich #71403) and histone octamer
524 was reconstituted and purified using published protocols (Luger et al. 1999a). Reconstituted octamers
525 were purified by size exclusion chromatography using a Superdex 200 Increase 10/300 GL column
526 (Cytiva #28990944). Nucleosomes were reconstituted using a 1:1.1 molar ratio of histone octamer to
527 DNA and purified by ion exchange chromatography following the protocol described (Luger et al.
528 1999b), then dialyzed into 20 mM HEPES, pH 7.4 with 50 mM KCl.
529

530 *HAT assay*

531 Histone acetyltransferase assays were performed in 20 µL reactions containing 225 nM purified
532 nucleosomes, 200 ng purified Jade1L/HBO1 complex, and 200 µM acetyl-CoA (Sigma #A2181)
533 ±250ng of Oct4 in 20 mM Tris pH 7.4, 40 mM KCl and 5mM $MgCl_2$. Reactions were incubated at 37°C
534 for 30 min. Reactions were quenched by the addition of 5.5 mL of 5X SDS-PAGE sample buffer.
535 Samples were boiled at 98°C for 10 min and analyzed by Western blot using specific antibodies. The
536 extent of acetylation was quantified by ImageJ software (National Institutes of Health).

537

538 *CryoEM and image processing*

539 The HBO1 complex was reconstituted at 1.5 µM final concentration in 20 mM HEPES, pH 7.4,
540 50 µM KCl and 1 mM DTT using individually purified HBO1, Jade1L, ING4 and hEaf6 from Sf9 cells
541 (ATCC #CRL-1711) and incubated over ice for 15 min. 1.5 µM of purified $Oct4^{S229D}$ was separately
542 combined with an equimolar amount of purified nucleosome core particles and incubated over ice for
543 15 min. The reconstituted HBO complex was then added to the Oct4/nucleosome complex and
544 incubated over ice for an additional 30 min. The reconstituted complex was then lightly crosslinked
545 using 0.01% (v/v) glutaraldehyde (Sigma) for 30 sec. Excess crosslinker was quenched using Tris-Cl
546 pH 7.5. The final complex was concentrated to ~0.5 mg/mL using a 0.5ml Amicon ultra-centrifugal
547 filter with a cutoff 10 kD (Sigma Millipore). 3.5 µL of concentrated complex was added to a glow-
548 discharged UltraAufoil Gold Holey Films (R1.2/1.3 300-mesh Au, EMS #Q350AR13A). After blotting
549 the grids for 4 sec at 4°C and 95% relative humidity, the samples was plunged into liquid ethane using
550 a Vitrobot Mark IV (ThermoFisher). CryoEM images were recorded using a Titan Krios 300 kV
551 microscope equipped with a Gutan K3 camera at 80000X magnification for a final pixel size 1.06
552 Å/pixel with a defocused range -0.8 to -1.8 µm using EPU data acquisition software (ThermoFisher).
553 Images were recorded under low-dose conditions with a total dose of ~ 60 electrons per $Å^2$ over 60
554 frames. A total of 6200 dose-fractionated image stacks were processed using CryoSPARC
555 4.0(Punjani et al. 2017). Images were corrected by Patch Motion Correction, then contrast transfer
556 function (CTF) was estimated by Patch CTF Estimation. The dose-fractionated image stacks were the
557 manually curated to improve the quality of data. Particles were then manually picked, and templates
558 were created for template-based particle picking using box size 380 $Å^3$. A total of 2×10^6 particles were
559 parsed into 2D classes. 100782 particles were selected from the 2D classes for *ab initio*
560 reconstruction, and a heterogeneous refinement was performed using the reconstructed 3D volume.
561 Each group of particles from heterogeneous refinement was taken for non-uniform (NU) refinement.
562 The best resolution obtained (gold-standard Fourier shell correlation, GSFSC) was 7.2 Å with a B
563 factor of 322. The volume map from the best resolution was smoothened using UCSF chimera at a
564 standard deviation of 1.5. The crystal structure of the Oct4 DNA binding domain bound to a MORE

565 (PDB ID: 7XRC) (Tan et al. 2023) and part of the nucleosome crystal structure (PDB ID: 6TEM) was
566 manually fitted using UCSF chimera. Part of the DNA from the same nucleosome was removed and
567 replaced with B-form DNA of the correct sequence generated separately using UCSF Chimera X. The
568 processed data have been uploaded to the Electron Microscopy Data Bank (EMDB, deposition code
569 EMD-47299).

570 **Competing interest statement**

571 The authors declare no competing interests.

572

573 **Acknowledgements**

574 We thank Jacques Cotê for the gift of the Jade1L expression construct. We thank J. Cox and the
575 Proteomics core facility for assistance with mass spectrometry. We thank B. Dalley and the High-
576 Throughput Sequencing Core facility, and T. Parnell and the Bioinformatics core facility for assistance
577 with ChIP-seq and analysis. We thank D. Belnap, B. Ganser-Pornillos and the Electron Microscopy
578 Core facility for assistance with cryoEM. We thank B. Cairns and members of his laboratory for the gift
579 of recombinant histone plasmid constructs. This work was supported by a grant from the NIH
580 (1R03TR004568) to DT.

581

582 *Author contributions:* D.T. conceived the study. Y.W., A.M. and D.T. designed experiments. Y.W.,
583 A.M., H.H. and M.B.C. generated new reagents for the study. Y.W., A.M., L.L. and M.B.C. performed
584 experiments and/or analyzed data. Y.W., A.M. and M.B.C. generated figures. All authors contributed
585 to the writing of the manuscript and read and approved the final version of the manuscript prior to
586 submission for publication.

587 **Figure Legends**

588 Figure 1. Oct4 DNA affinity purification identifies Jade1 as a spatioselective interaction partner. (*A*)
589 Bead affinity capture workflow. Oct1 deficient ES cell lysates were incubated wild-type or mutant
590 octamer or MORE DNA sequences immobilized on FG beads. Proteins were eluted using high salt
591 and free excess DNA, and the eluates are then verified by Western Blot and analyzed by mass
592 spectrometry. (*B*) Material eluted from (A) was immunoblotted using Oct4 antibodies as a quality
593 control. (*C*) MS-Mascot output showing the 58 proteins enriched using wild-type octamer relative to
594 mutant DNA. Average fold enrichment vs. negative inverse log10 *p*-value is shown based on N=3
595 independent experiments. Threshold lines show 2-fold enrichment and *p*=.05. Black text indicates
596 proteins identified in prior studies. Red text shows POU proteins. Octamer-binding POU transcription
597 factor proteins are shown in red. (*D*) Similar analysis using MORE DNA. 27 proteins were significantly
598 enriched.

599

600 Figure 2. Oct4 interacts with Jade1. (*A*) Oct4 and its cofactors in Oct1 deficient ESCs were
601 precipitated using FG beads immobilized with wild-type or mutant octamer and MORE DNA
602 sequences. The isolated material was immunoblotted using Oct4 and Jade1 antibodies. (*B*) Extracts
603 from Oct1 deficient ESCs were used for immunoprecipitation with Jade1 antibody or corresponding
604 rabbit IgG as negative control and immunoblotted with Oct4 antibody. (*C*) Oct1 deficient ESCs were
605 immunoprecipitated with Oct4 antibody and corresponding mouse IgG as negative control and
606 immunoblotted with Jade1 antibodies. (*D*) 3T3 cells were transfected with plasmids encoding FLAG-
607 and twin-strep-tagged Oct4 or ΔN Oct4 using Lipofectamine 3000. After 48 hr, cells fixed and stained
608 with antibodies against Oct4 (Donkey anti-mouse Oct4-Alexa 488) and imaged using an EVOS
609 M7000 microscope. (*E*) Expi293F cells were transiently transfected with plasmids encoding FLAG-
610 and twin-strep-tagged Oct4 or ΔN Oct4, and twin-strep-tagged Jade1L. After 48 hr, lysates were
611 prepared in the presence of MG-132 and incubated with MORE DNA-coupled FG beads, washed,
612 resolved using SDS-PAGE and probed with anti-StrepII antibodies-HRP.

613

614 Figure 3. Jade1/HBO1 complex prefer binding at MORE sites compared to Octamer sites. (*A*) Venn
615 diagram showing Oct4 ChIP peaks and HBO1 ChIP peaks and overlapping peaks. (*B*) HBO1 ChIP
616 peaks and Oct4 ChIP peaks at example MOREs (*Polr2a*, *Zmiz2* and *Rras2*) and the octamer site
617 (*Pou5f1*). (*C*) Motif identification using MEME-ChIP at Oct4 and HBO1 overlapping ChIP peaks.

618

619 Figure 4. Oct4 augments acetylation of histone H3K9 by the HBO1/Jade1L complex. (*A*) Histone
620 Acetyl Transferase (HAT) assay using nucleosome core particles (NCPs) containing a MORE near
621 the entry/exit site. NCPs were treated with purified Jade1L complex in the presence or absence of
622 Oct4. NCP alone was included as a control (lane 1). Reactions were immunoblotted with antibodies

623 against acetylated histone H4. Pan-H3 antibodies were included as a loading control. (*B*) Acetylation
624 of specific histone H4 and H3 tail lysines was detected by immunoblotting. (*C*) Quantitation of
625 acetylation of specific histone lysines by the HBO1/Jade1L complex in the absence or presence of
626 Oct4. Quantitation was performed using Image J software from N=3 independent experiments. Error
627 bars indicate standard deviation. Data were plotted using GraphPad Prism software.
628
629 Figure 5. An Oct4 mutant that more efficiently binds to MOREs more efficiently acetylates
630 nucleosomes in the presence of the HBO1/Jade1L complex. (*A*) EMSA showing Oct4 protein binding
631 to Cy5-labeled MORE DNA probe with or without the Jade1L/HBO1 HAT complex. Monomeric and
632 dimeric interactions with the DNA are indicated by the arrows. (*B*) Comparison of increasing
633 concentrations of wild-type and S229D Oct4 binding to a MORE DNA probe. Monomeric and dimeric
634 interactions bands are also shown by the arrow. (*C*) HAT assay using MORE-containing nucleosome
635 core particles (NCPs) treated with 200 ng purified Jade1L complex in the presence of increasing
636 amounts of purified Oct4 wild-type and mutant proteins. The extent of histone H3K9 acetylation was
637 detected by Western blotting.
638
639 Figure 6. Structural analysis of Oct4 bound to a MORE complexed with HBO1/Jade1 HAT and
640 nucleosome. (*A*) 153-bp DNA sequence used for nucleosome preparation. The position of the MORE
641 is indicated in red. (*B*) Representative micrograph collected by cryoEM. (*C*) Selected 2D classes are
642 shown. (*D*) 3D-reconstructed and refined volume for the HBO1/Jade1/ING4/hEaaf6/Oct4/nucleosome
643 complex is shown in two projections rotated 90°. (*E*) Two copies of the Oct4 DNA binding domains
644 (POU_S and POU_H, PDB ID: 7XRC) were fitted in the extended volume. Positions of the two DBD N-
645 and C-termini are highlighted. (*F*) Partial structure of the nucleosome (PDB ID: 6TEM) fitted within the
646 volume. Part of the DNA was opened and fitted into the extended volume where the predicted location
647 of the MORE is shown in red. Left and right panels were rotated 90°.
648
649
650 **Supplemental Figure Legends**
651 Supplemental Figure S1. (*A*) Venn diagram comparing unique and common identified proteins
652 enriched using affinity purification with octamer compared to MORE DNA. Percentage of protein hits
653 that are unique to the two conditions are shown. Example proteins from each of the three groups are
654 shown. (*B*) The union of all identified proteins enriched using octamer or MORE affinity purification (78
655 total proteins) was compared with proteins identified from three prior studies (Pardo et al. 2010; van
656 den Berg et al. 2010; Ding et al. 2012). Proteins previously identified in the different studies are

657 shown. Bold text indicates proteins selectively enriched using MORE DNA in (A). Figure adapted from
658 Ding et al., 2011.
659
660 Supplemental Figure S2. Further validation of the selective interaction of Jade1L and Oct4 on MORE-
661 containing DNA. (*A*) Oct4 and its cofactors in Oct1 deficient ESCs were precipitated using FG beads
662 immobilized with wild-type or mutant octamer and MORE DNA sequences was immunoblotted using
663 Oct4 and Jade1 antibodies in a second biological repeat of the data shown in Figure 2A. The upper
664 panel shows a strong exposure, and the lower panel shows a light exposure. (*B*) Wild-type ESCs
665 were immunoprecipitated with an Oct4 antibody and corresponding mouse IgG as negative control
666 and immunoblotted with Jade1 antibodies.
667
668 Supplemental Figure S3. Characterization of HBO1 binding events in ESCs. (*A*) Analysis of HBO1
669 ChIP peak genomic locations. (*B*) HBO1 ChIP peaks intensities were aligned based on transcription
670 start site (TSS) and plotted based on ±distance from TSS. (*C*) The distance between Oct4 and HBO1
671 ChIP-seq peak centers was calculated for all common genes, and for MORE-containing genes
672 (*Polr2a*, *Zmiz*, two peaks in *Blacap*, and *Rras2*). The average internal is plotted with mean and ±SEM.
673
674 Supplemental Figure S4. Purification of recombinant components of the HBO1 complex. (*A*) Individual
675 proteins were overexpressed in Expi293F cells and purified using their FLAG tags. The purified
676 proteins were analyzed by 12% SDS-PAGE and Coomassie staining. Arrow indicates the position of
677 the specific protein. (*B*) Proteins copurifying with Jade1L were confirmed by Western blot using the
678 corresponding antibodies. (*C*) Sequence alignment of human Oct1 (accession number: AAH52274.1)
679 and Oct4 (accession number: NP_038661.2) is shown. Red rectangle indicates S385 in Oct1, which
680 corresponds to position S229 in Oct4.
681
682 Supplemental Figure S5. Recombinant protein purification of Jade1L, HBO1, ING4 and hEaf6. (*A*)
683 Jade1L and HBO1 were independently purified from sf9 cells using their twin-strep tags. Purified
684 proteins were analyzed on 12% SDS-PAGE gel. Arrows indicate the position of the specific protein in
685 the Coomassie stained gels. (*B*) Similar purification of ING4 and hEaf6. $Oct4^{S229D}$ used in cryoEM was
686 overexpressed and purified from Expi293F cells using FLAG tags.
687
688 Supplemental Figure S6. Workflow for cyro-EM analysis. (*A*) Schematics for cryoEM data analysis
689 using CryoSPARC. The number of the particles and resolution are shown under each group. (*B*) Real
690 space slices are shown for the corresponding NU refinement. (*C*) GSFSC resolution plots are shown

691 for the corresponding NU refinement. (*D*) viewing direction distributions are shown for the
692 corresponding NU refinement.
693
694 Supplemental Figure S7. Model for spatioselective recruitment of Jade1 and HBO1 by multimeric
695 Oct4 at nucleosomes to acetylate H3K9. (*A*) At typical binding sides, Oct4 recruits more generic
696 cofactors (X and Y) to regulate transcription either positively or negatively. (*B*) At MORE sites, dimeric
697 Oct4 associates with Jade1 and the HBO1 HAT complex to acetylate H3K9 at local nucleosomes.
698 Other components of the complex such as Eaf6 and ING4 are also shown.

References

Ambrosetti DC, Basilico C, Dailey L. 1997. Synergistic activation of the fibroblast growth factor 4 enhancer by Sox2 and Oct-3 depends on protein-protein interactions facilitated by a specific spatial arrangement of factor binding sites. *Mol Cell Biol* **17**: 6321-6329.

Bekere I, de Oliveira Mann CC. 2022. FoxP3 forkhead dimer: Don't swap me now. *Immunity* **55**: 1329-1331.

Boija A, Klein IA, Sabari BR, Dall'Agnese A, Coffey EL, Zamudio AV, Li CH, Shrinivas K, Manteiga JC, Hannett NM et al. 2018. Transcription Factors Activate Genes through the Phase-Separation Capacity of Their Activation Domains. *Cell* **175**: 1842-1855.e1816.

Botquin V, Hess H, Fuhrmann G, Anastassiadis C, Gross MK, Vriend G, Schöler HR. 1998. New POU dimer configuration mediates antagonistic control of an osteopontin preimplantation enhancer by Oct-4 and Sox-2. *Genes Dev* **12**: 2073-2090.

Brumbaugh J, Hou Z, Russell JD, Howden SE, Yu P, Ledvina AR, Coon JJ, Thomson JA. 2012. Phosphorylation regulates human OCT4. *Proc Natl Acad Sci U S A* **109**: 7162-7168.

Campos EI, Reinberg D. 2009. Histones: annotating chromatin. *Annu Rev Genet* **43**: 559-599.

Chew JL, Loh YH, Zhang W, Chen X, Tam WL, Yeap LS, Li P, Ang YS, Lim B, Robson P et al. 2005. Reciprocal transcriptional regulation of Pou5f1 and Sox2 via the Oct4/Sox2 complex in embryonic stem cells. *Mol Cell Biol* **25**: 6031-6046.

Chinnadurai G. 2009. The transcriptional corepressor CtBP: a foe of multiple tumor suppressors. *Cancer Res* **69**: 731-734.

Ding J, Xu H, Faiola F, Ma'ayan A, Wang J. 2012. Oct4 links multiple epigenetic pathways to the pluripotency network. *Cell Res* **22**: 155-167.

Ferraris L, Stewart AP, Kang J, DeSimone AM, Gemberling M, Tantin D, Fairbrother WG. 2011. Combinatorial binding of transcription factors in the pluripotency control regions of the genome. *Genome Res* **21**: 1055-1064.

Foy RL, Song IY, Chitalia VC, Cohen HT, Saksouk N, Cayrou C, Vaziri C, Cote J, Panchenko MV. 2008. Role of Jade-1 in the histone acetyltransferase (HAT) HBO1 complex. *J Biol Chem* **283**: 28817-28826.

Gaurav N, Kanai A, Lachance C, Cox KL, Liu J, Grzybowski AT, Saksouk N, Klein BJ, Komata Y, Asada S et al. 2024. Guiding the HBO1 complex function through the JADE subunit. *Nat Struct Mol Biol* **31**: 1039-1049.

Han J, Lachance C, Ricketts MD, McCullough CE, Gerace M, Black BE, Cote J, Marmorstein R. 2018. The scaffolding protein JADE1 physically links the acetyltransferase subunit HBO1 with its histone H3-H4 substrate. *J Biol Chem* **293**: 4498-4509.

Herr W, Sturm RA, Clerc RG, Corcoran LM, Baltimore D, Sharp PA, Ingraham HA, Rosenfeld MG, Finney M, Ruvkun G. 1988. The POU domain: a large conserved region in the mammalian pit-1, oct-1, oct-2, and Caenorhabditis elegans unc-86 gene products. *Genes Dev* **2**: 1513-1516.

Isshiki Y, Iwama A. 2018. Emerging role of noncanonical polycomb repressive complexes in normal and malignant hematopoiesis. *Exp Hematol* **68**: 10-14.

Kang J, Gemberling M, Nakamura M, Whitby FG, Handa H, Fairbrother WG, Tantin D. 2009. A general mechanism for transcription regulation by Oct1 and Oct4 in response to genotoxic and oxidative stress. *Genes Dev* **23**: 208-222.

Kim KP, Han DW, Kim J, Scholer HR. 2021. Biological importance of OCT transcription factors in reprogramming and development. *Exp Mol Med* **53**: 1018-1028.

King HW, Klose RJ. 2017. The pioneer factor OCT4 requires the chromatin remodeller BRG1 to support gene regulatory element function in mouse embryonic stem cells. *Elife* **6**.

Klemm JD, Rould MA, Aurora R, Herr W, Pabo CO. 1994. Crystal structure of the Oct-1 POU domain bound to an octamer site: DNA recognition with tethered DNA-binding modules. *Cell* **77**: 21-32.

Lalonde ME, Avvakumov N, Glass KC, Joncas FH, Saksouk N, Holliday M, Paquet E, Yan K, Tong Q, Klein BJ et al. 2013. Exchange of associated factors directs a switch in HBO1 acetyltransferase histone tail specificity. *Genes Dev* **27**: 2009-2024.

751 Liang J, Wan M, Zhang Y, Gu P, Xin H, Jung SY, Qin J, Wong J, Cooney AJ, Liu D et al. 2008. Nanog
752 and Oct4 associate with unique transcriptional repression complexes in embryonic stem cells.
753 *Nat Cell Biol* **10**: 731-739.
754 Lis JT, Schleif R. 1975. Size fractionation of double-stranded DNA by precipitation with polyethylene
755 glycol. *Nucleic Acids Res* **2**: 383-389.
756 Luger K, Rechsteiner TJ, Richmond TJ. 1999a. Expression and purification of recombinant histones
757 and nucleosome reconstitution. *Methods Mol Biol* **119**: 1-16.
758 -. 1999b. Preparation of nucleosome core particle from recombinant histones. *Methods Enzymol* **304**:
759 3-19.
760 Marmorstein R, Roth SY. 2001. Histone acetyltransferases: function, structure, and catalysis. *Curr*
761 *Opin Genet Dev* **11**: 155-161.
762 Martire S, Banaszynski LA. 2020. The roles of histone variants in fine-tuning chromatin organization
763 and function. *Nat Rev Mol Cell Biol* **21**: 522-541.
764 Michael AK, Grand RS, Isbel L, Cavadini S, Kozicka Z, Kempf G, Bunker RD, Schenk AD, Graff-
765 Meyer A, Pathare GR et al. 2020. Mechanisms of OCT4-SOX2 motif readout on nucleosomes.
766 *Science* **368**: 1460-1465.
767 Nair S, Ameen M, Sundaram L, Pampari A, Schreiber J, Balsubramani A, Wang YX, Burns D, Blau
768 HM, Karakikes I et al. 2023. Transcription factor stoichiometry, motif affinity and syntax
769 regulate single-cell chromatin dynamics during fibroblast reprogramming to pluripotency.
770 *bioRxiv*.
771 Nishi M, Akutsu H, Masui S, Kondo A, Nagashima Y, Kimura H, Perrem K, Shigeri Y, Toyoda M,
772 Okayama A et al. 2011. A distinct role for Pin1 in the induction and maintenance of
773 pluripotency. *J Biol Chem* **286**: 11593-11603.
774 Ogryzko VV, Schiltz RL, Russanova V, Howard BH, Nakatani Y. 1996. The transcriptional
775 coactivators p300 and CBP are histone acetyltransferases. *Cell* **87**: 953-959.
776 Oka M, Moriyama T, Asally M, Kawakami K, Yoneda Y. 2013. Differential role for transcription factor
777 Oct4 nucleocytoplasmic dynamics in somatic cell reprogramming and self-renewal of
778 embryonic stem cells. *J Biol Chem* **288**: 15085-15097.
779 Pang Z, Chong J, Zhou G, de Lima Morais DA, Chang L, Barrette M, Gauthier C, Jacques P, Li S, Xia
780 J. 2021. MetaboAnalyst 5.0: narrowing the gap between raw spectra and functional insights.
781 *Nucleic Acids Res* **49**: W388-W396.
782 Pardo M, Lang B, Yu L, Prosser H, Bradley A, Babu MM, Choudhary J. 2010. An expanded Oct4
783 interaction network: implications for stem cell biology, development, and disease. *Cell Stem*
784 *Cell* **6**: 382-395.
785 Perovanovic J, Wu Y, Abewe H, Shen Z, Hughes EP, Gertz J, Chandrasekharan MB, Tantin D. 2023.
786 Oct1 cooperates with the Smad family of transcription factors to promote mesodermal lineage
787 specification. *Sci Signal* **16**: eadd5750.
788 Pesce M, Schöler HR. 2001. Oct-4: gatekeeper in the beginnings of mammalian development. *Stem*
789 *Cells* **19**: 271-278.
790 Punjani A, Rubinstein JL, Fleet DJ, Brubaker MA. 2017. cryoSPARC: algorithms for rapid
791 unsupervised cryo-EM structure determination. *Nat Methods* **14**: 290-296.
792 Remenyi A, Tomilin A, Pohl E, Lins K, Philippsen A, Reinbold R, Scholer HR, Wilmanns M. 2001.
793 Differential dimer activities of the transcription factor Oct-1 by DNA-induced interface
794 swapping. *Mol Cell* **8**: 569-580.
795 Shakya A, Callister C, Goren A, Yosef N, Garg N, Khoddami V, Nix D, Regev A, Tantin D. 2015a.
796 Pluripotency transcription factor Oct4 mediates stepwise nucleosome demethylation and
797 depletion. *Mol Cell Biol* **35**: 1014-1025.
798 Shakya A, Goren A, Shalek A, German CN, Snook J, Kuchroo VK, Yosef N, Chan RC, Regev A,
799 Williams MA et al. 2015b. Oct1 and OCA-B are selectively required for CD4 memory T cell
800 function. *J Exp Med* **212**: 2115-2131.
801 Shen Z, Kang J, Shakya A, Tabaka M, Jarboe EA, Regev A, Tantin D. 2017. Enforcement of
802 developmental lineage specificity by transcription factor Oct1. *Elife* **6**.

803 Shen Z, Wu Y, Manna A, Yi C, Cairns BR, Evason KJ, Chandrasekharan MB, Tantin D. 2024. Oct4
804 redox sensitivity potentiates reprogramming and differentiation. *Genes Dev* **38**: 308-321.
805 Sinha K, Bilokapic S, Du Y, Malik D, Halic M. 2023a. Histone modifications regulate pioneer
806 transcription factor binding and cooperativity. *bioRxiv*.
807 Sinha KK, Bilokapic S, Du Y, Malik D, Halic M. 2023b. Histone modifications regulate pioneer
808 transcription factor cooperativity. *Nature* **619**: 378-384.
809 Stadhouders R, Vidal E, Serra F, Di Stefano B, Le Dily F, Quilez J, Gomez A, Collombet S, Berenguer
810 C, Cuartero Y et al. 2018. Transcription factors orchestrate dynamic interplay between
811 genome topology and gene regulation during cell reprogramming. *Nat Genet* **50**: 238-249.
812 Tan DS, Cheung SL, Gao Y, Weinbuch M, Hu H, Shi L, Ti SC, Hutchins AP, Cojocaru V, Jauch R.
813 2023. The homeodomain of Oct4 is a dimeric binder of methylated CpG elements. *Nucleic*
814 *Acids Res* **51**: 1120-1138.
815 Tantin D. 2013. Oct transcription factors in development and stem cells: insights and mechanisms.
816 *Development* **140**: 2857-2866.
817 Tantin D, Gemberling M, Callister C, Fairbrother WG. 2008. High-throughput biochemical analysis of
818 in vivo location data reveals novel distinct classes of POU5F1(Oct4)/DNA complexes. *Genome*
819 *Res* **18**: 631-639.
820 Tomilin A, Reményi A, Lins K, Bak H, Leidel S, Vriend G, Wilmanns M, Schöler HR. 2000. Synergism
821 with the coactivator OBF-1 (OCA-B, BOB-1) is mediated by a specific POU dimer
822 configuration. *Cell* **103**: 853-864.
823 Utley RT, Côté J. 2003. The MYST family of histone acetyltransferases. *Curr Top Microbiol Immunol*
824 **274**: 203-236.
825 van den Berg DL, Snoek T, Mullin NP, Yates A, Bezstarosti K, Demmers J, Chambers I, Poot RA.
826 2010. An Oct4-centered protein interaction network in embryonic stem cells. *Cell Stem Cell* **6**:
827 369-381.
828 Wade PA, Wolffe AP. 1997. Histone acetyltransferases in control. *Curr Biol* **7**: R82-84.
829 Wu C, Read C, McGeehan J, Crane-Robinson C. 2016. The construction of customized nucleosomal
830 arrays. *Anal Biochem* **496**: 71-75.
831 Xiao Y, Li W, Yang H, Pan L, Zhang L, Lu L, Chen J, Wei W, Ye J, Li J et al. 2021. HBO1 is a
832 versatile histone acyltransferase critical for promoter histone acylations. *Nucleic Acids Res* **49**:
833 8037-8059.
834 Ye Y, Wu H, Chen K, Clapier CR, Verma N, Zhang W, Deng H, Cairns BR, Gao N, Chen Z. 2019.
835 Structure of the RSC complex bound to the nucleosome. *Science* **366**: 838-843.
836 Zhang C, Shan Y, Lin H, Zhang Y, Xing Q, Zhu J, Zhou T, Lin A, Chen Q, Wang J et al. 2024. HBO1
837 determines SMAD action in pluripotency and mesendoderm specification. *Nucleic Acids Res*
838 **52**: 4935-4949.
839 Zhou MI, Wang H, Ross JJ, Kuzmin I, Xu C, Cohen HT. 2002. The von Hippel-Lindau tumor
840 suppressor stabilizes novel plant homeodomain protein Jade-1. *J Biol Chem* **277**: 39887-
841 39898.
842

Wu, Manna et al. Fig. 1

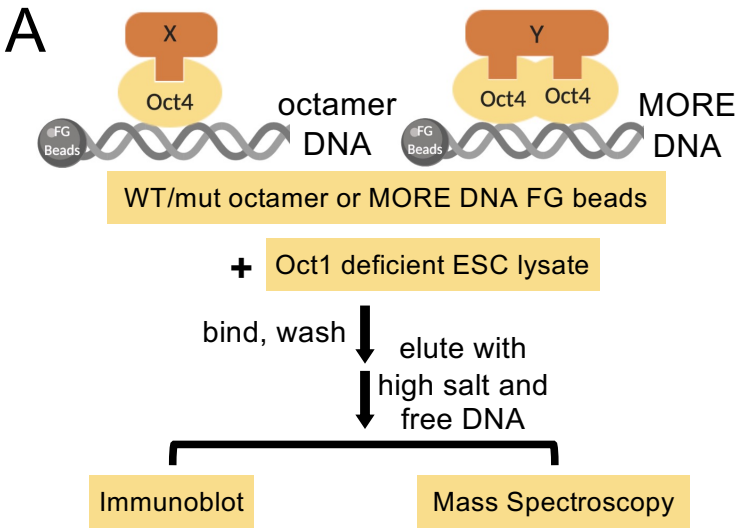

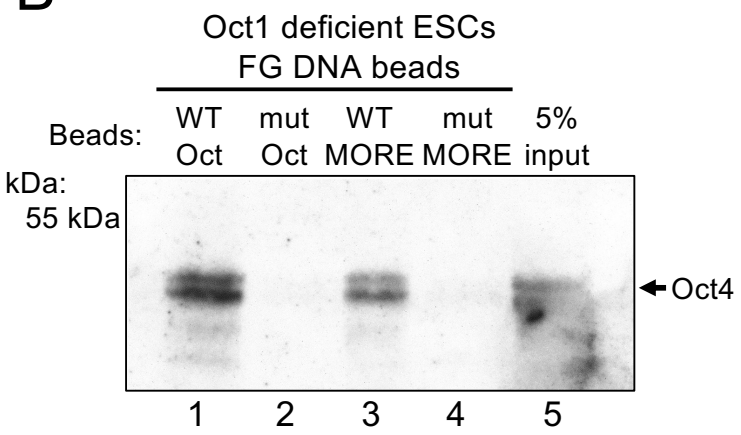

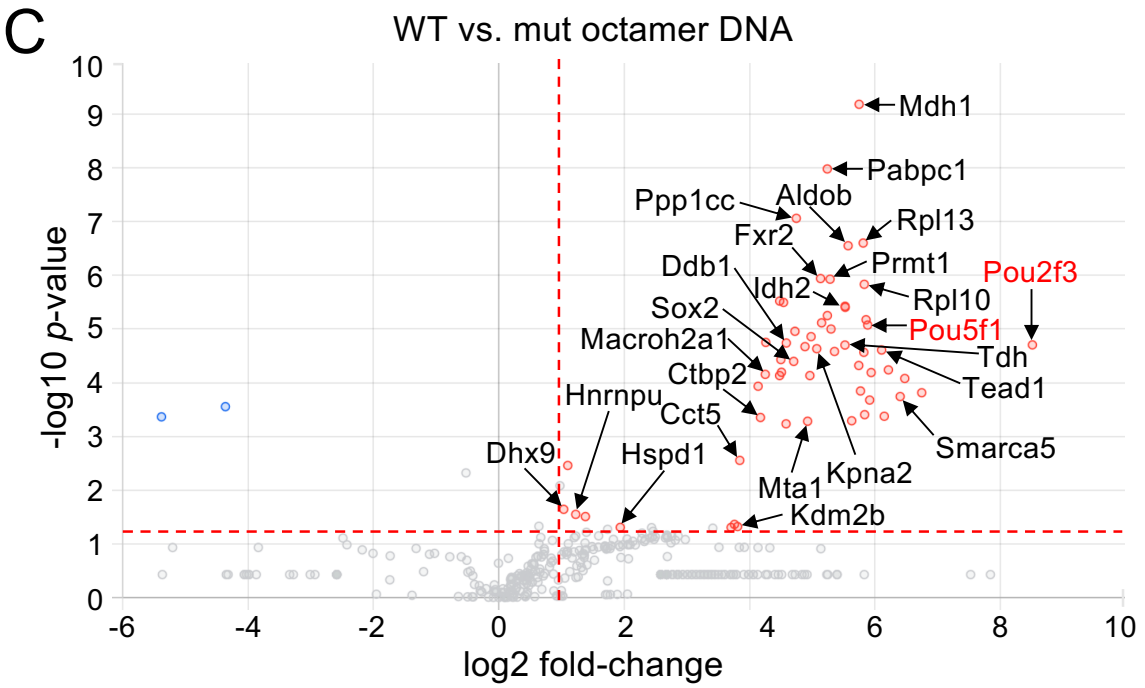

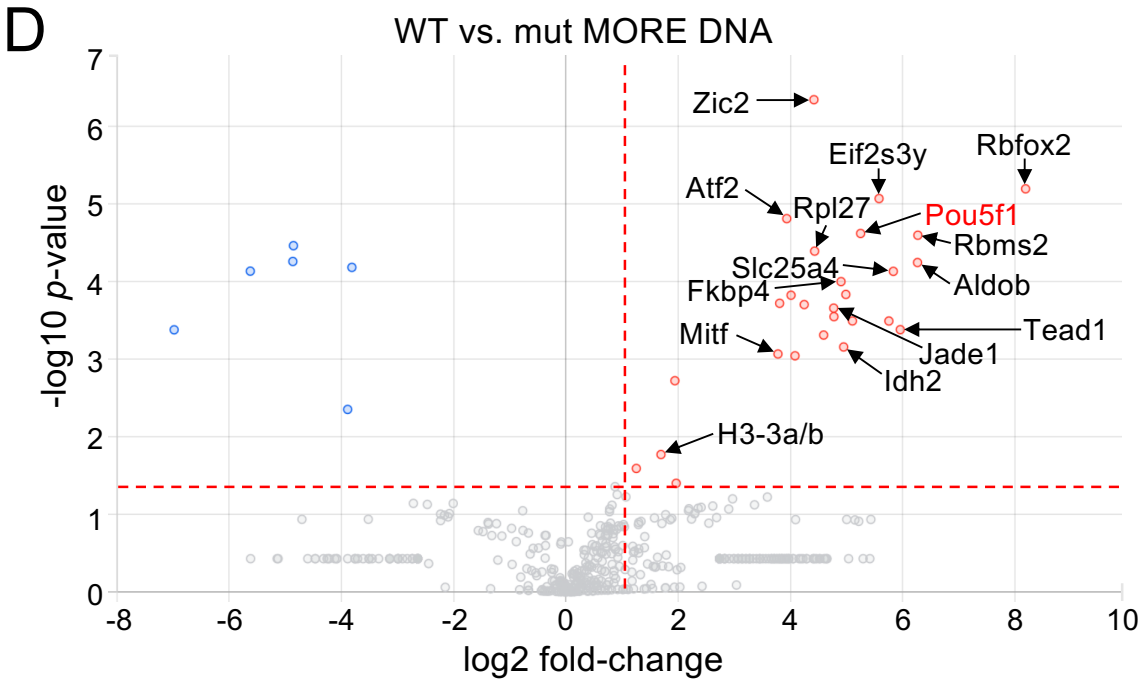

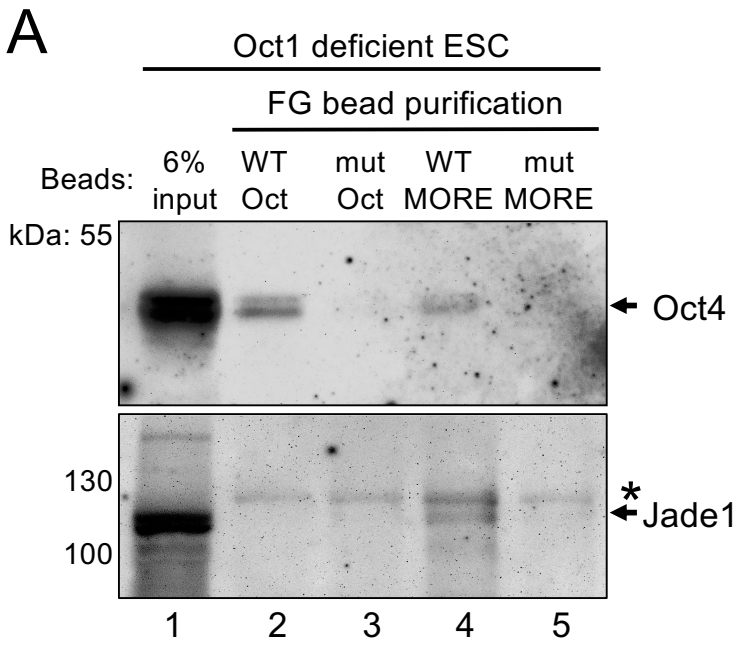
A
Oct1 deficient ESC
FG bead purification
Beads:
6% input
WT Oct
mut Oct
WT MORE
mut MORE
kDa: 55
Oct4
130
100
*
Jade1
1
2
3
4
5

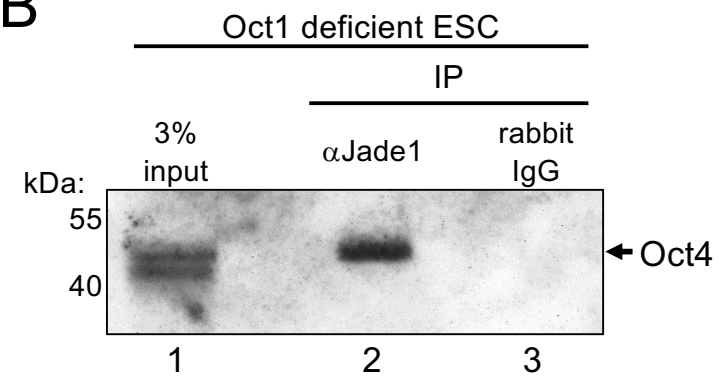
B
Oct1 deficient ESC
IP
3% input
αJade1
rabbit IgG
kDa:
55
40
Oct4
1
2
3

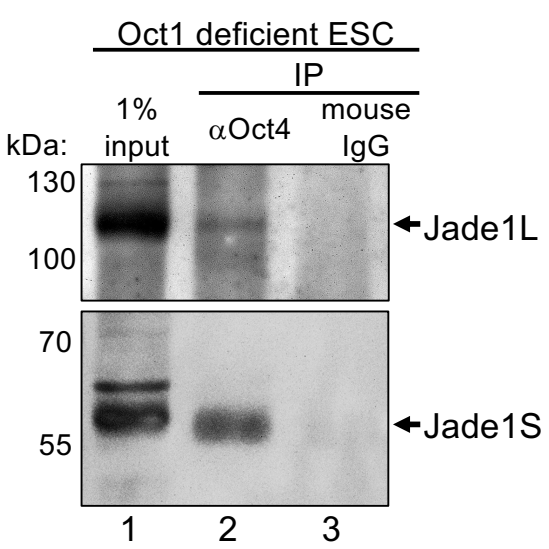
C
Oct1 deficient ESC
IP
1% input
αOct4
mouse IgG
kDa:
130
100
Jade1L
70
55
Jade1S
1
2
3

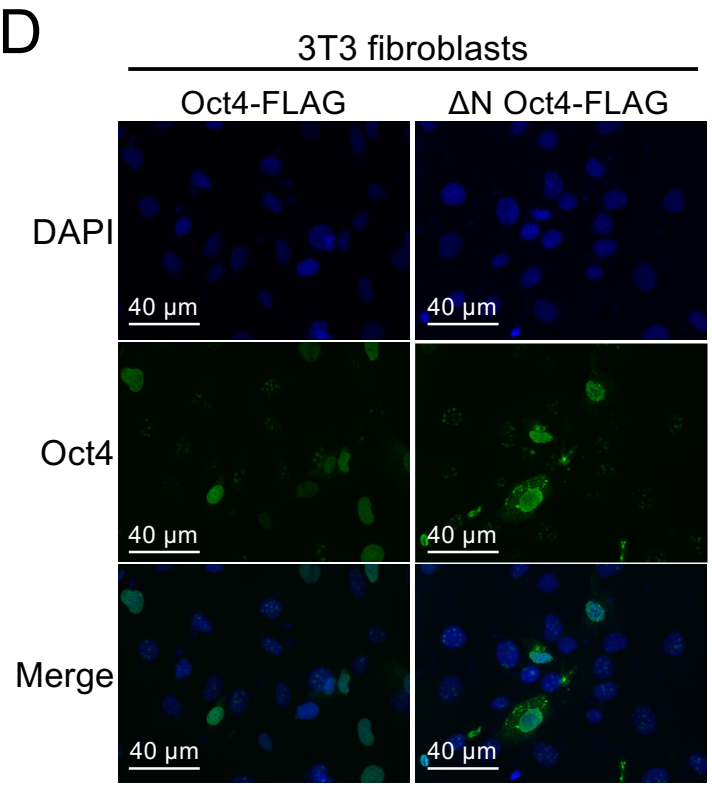
D
3T3 fibroblasts
Oct4-FLAG
ΔN Oct4-FLAG
DAPI
Oct4
Merge
40 μm

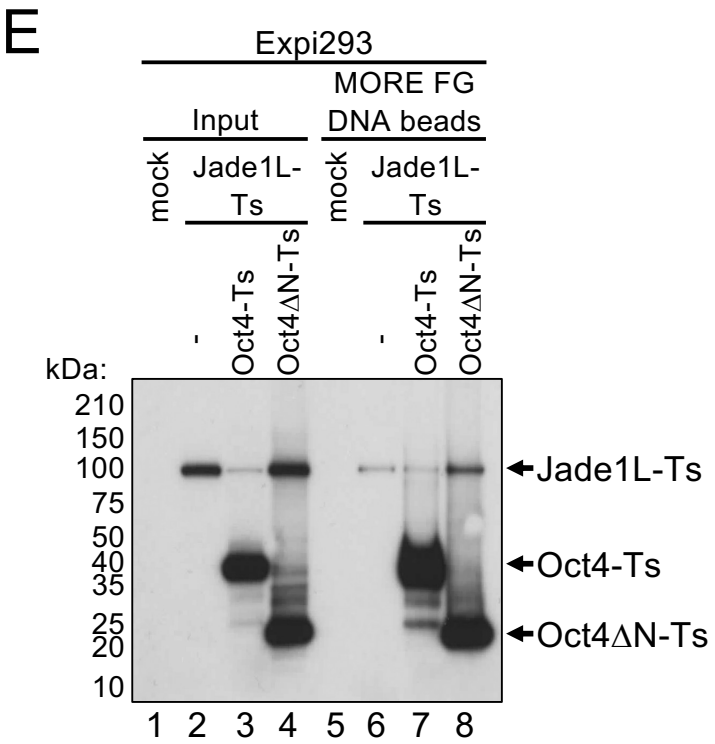
E
Expi293
Input
MORE FG DNA beads
mock
Jade1L-Ts
-
Oct4-Ts
Oct4ΔN-Ts
kDa:
210
150
100
75
50
40
35
25
20
10
Jade1L-Ts
Oct4-Ts
Oct4ΔN-Ts
1
2
3
4
5
6
7
8

Wu, Manna et al. Fig. 3

A

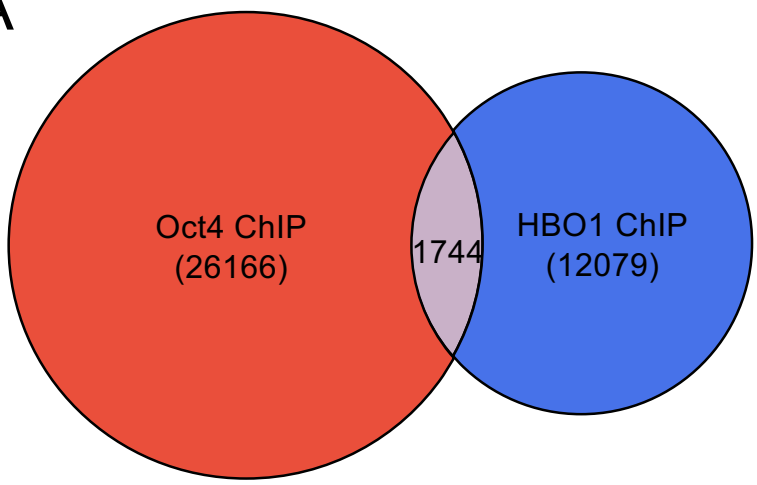

B

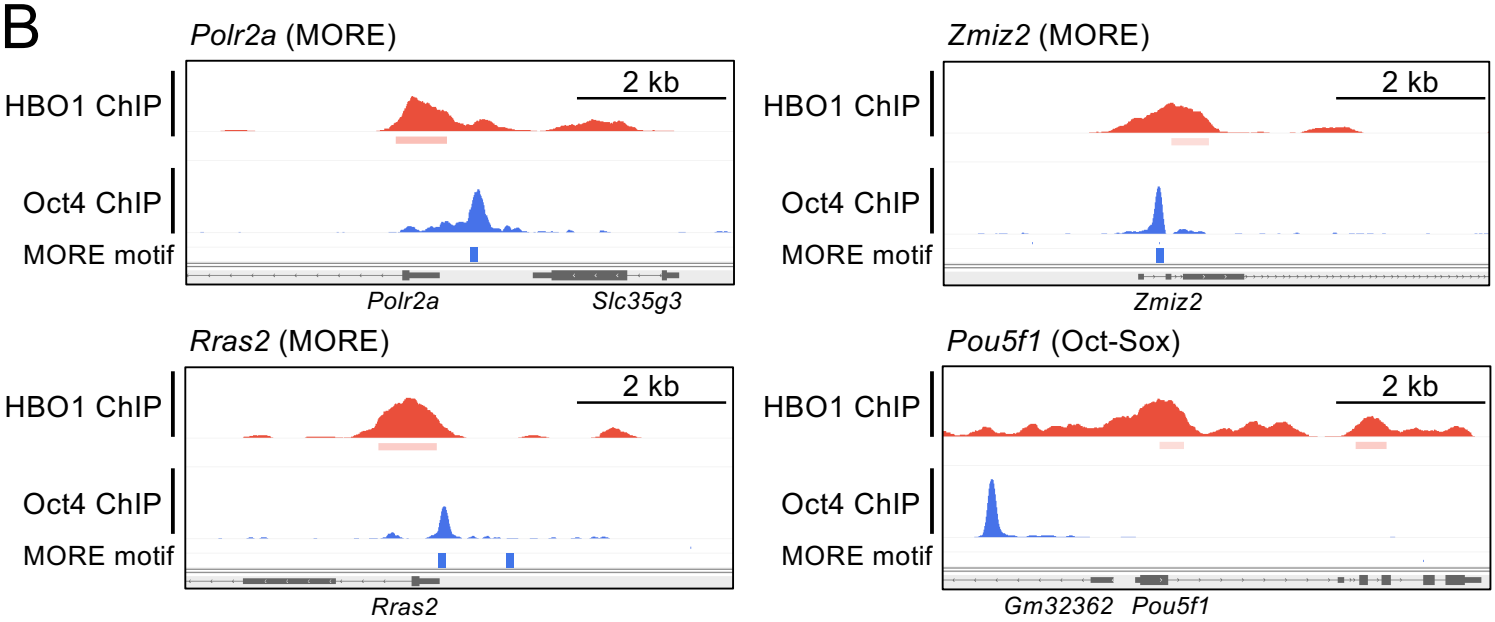

C

Top motifs identified in Oct4/HBO1 peaks:

de novo motifs	Oct4/HBO1 (1744 peaks)
1. (MORE)	*E*=6e-10
2. (octamer)	*E*=3.2e-9

Top motifs identified in Oct4 peaks alone:

de novo motifs	Oct4 (12079 peaks)
1. (octamer)	*E*=6.5e-447
2. (MORE)	*E*=1.4e-237

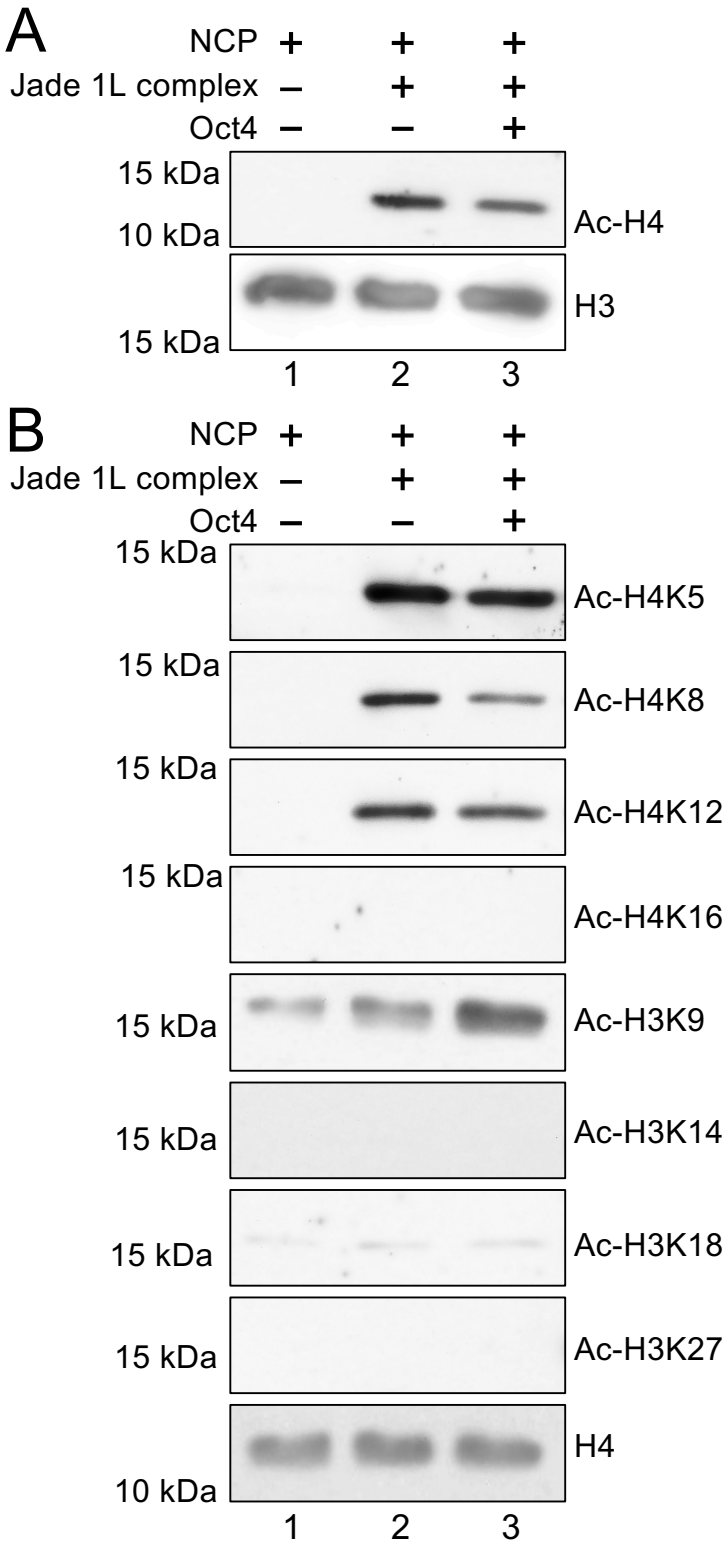
A
NCP + + +
Jade 1L complex – + +
Oct4 – – +
15 kDa
10 kDa
Ac-H4
H3
15 kDa
1 2 3
B
NCP + + +
Jade 1L complex – + +
Oct4 – – +
15 kDa
Ac-H4K5
15 kDa
Ac-H4K8
15 kDa
Ac-H4K12
15 kDa
Ac-H4K16
15 kDa
Ac-H3K9
15 kDa
Ac-H3K14
15 kDa
Ac-H3K18
15 kDa
Ac-H3K27
H4
10 kDa
1 2 3

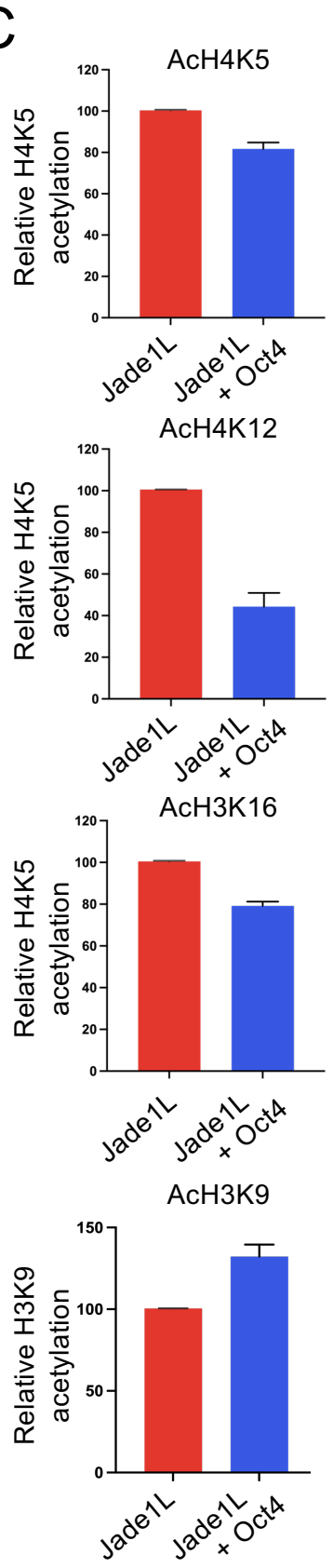
C
AcH4K5
Relative H4K5 acetylation
0 20 40 60 80 100 120
Jade1L
Jade1L + Oct4
AcH4K12
Relative H4K5 acetylation
0 20 40 60 80 100 120
Jade1L
Jade1L + Oct4
AcH3K16
Relative H4K5 acetylation
0 20 40 60 80 100 120
Jade1L
Jade1L + Oct4
AcH3K9
Relative H3K9 acetylation
0 50 100 150
Jade1L
Jade1L + Oct4

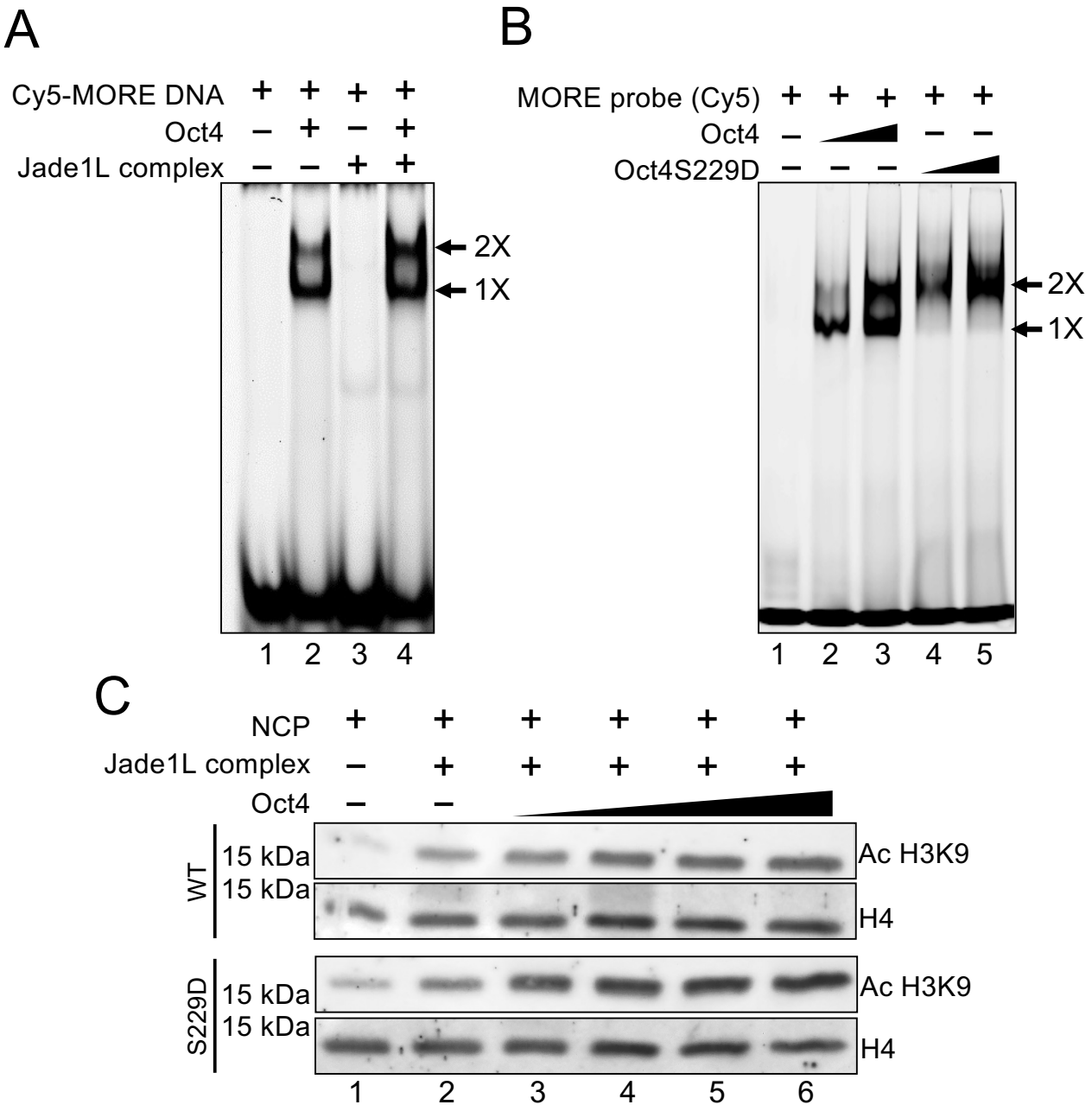
A
Cy5-MORE DNA + + + +
Oct4 – + – +
Jade1L complex – – + +
2X
1X
1 2 3 4
B
MORE probe (Cy5) + + + + +
Oct4 –
Oct4S229D – – –
2X
1X
1 2 3 4 5
C
NCP + + + + + +
Jade1L complex – + + + + +
Oct4 – –
WT
15 kDa
15 kDa
Ac H3K9
H4
S229D
15 kDa
15 kDa
Ac H3K9
H4
1 2 3 4 5 6

Wu, Manna et al. Fig. 6

A

MORE

5'ATCCTGGAGAAATGCATATGCATGGCCGCTCAATTGGTCGTAGACAGCTCT
3'TAGGACCTCTTTACGTATACGTACCGGCGAGTTAACCAGCATCTGTCGAGA
10 20 30 40 50

AGCACCGCTTAAACGCACGTACGCGCTGTCCCCCGCGTTTTAACCGCCAAG
TCGTGGCGAATTTGCGTGCATGCGCGACAGGGGGCGCAAAATTGGCGGTTC
60 70 80 90 100

GGGATTACTCCCTAGTCTCCAGGCACGTGTCAGATATATACATCCTGTGAT3'
CCCTAATGAGGGATCAGAGGTCCGTGCACAGTCTATATATGTAGGACACTA5'
110 120 130 140 150

B

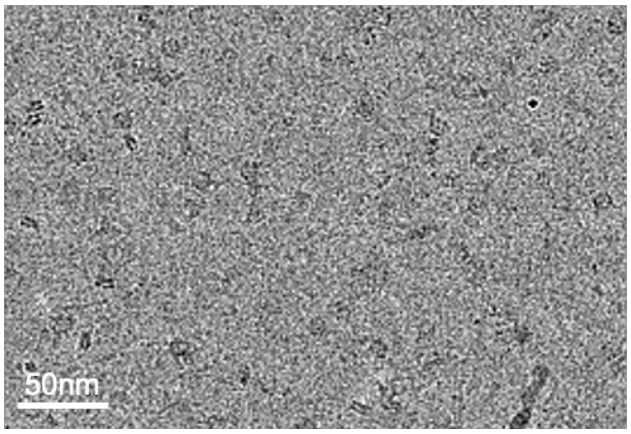

C

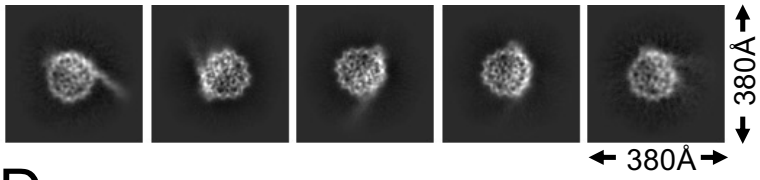

D

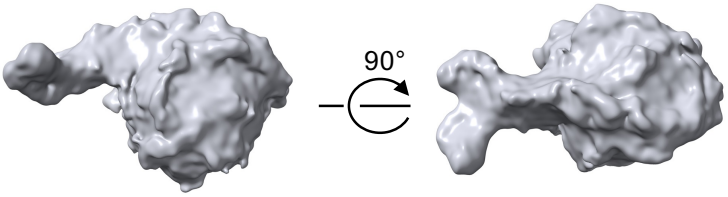

E

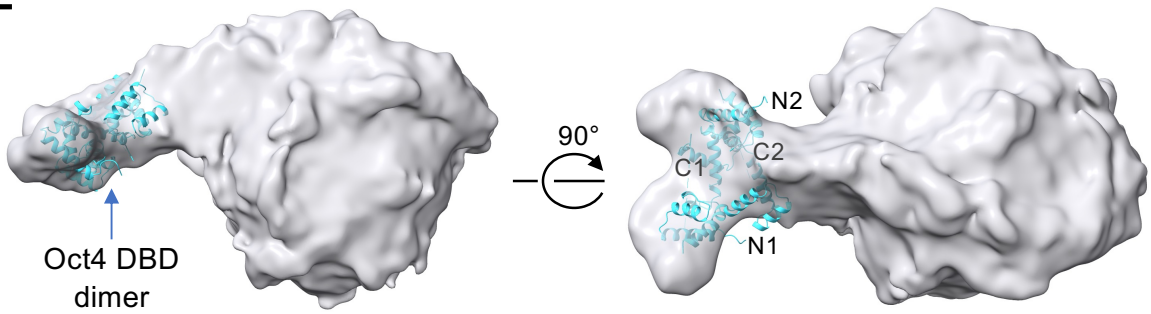
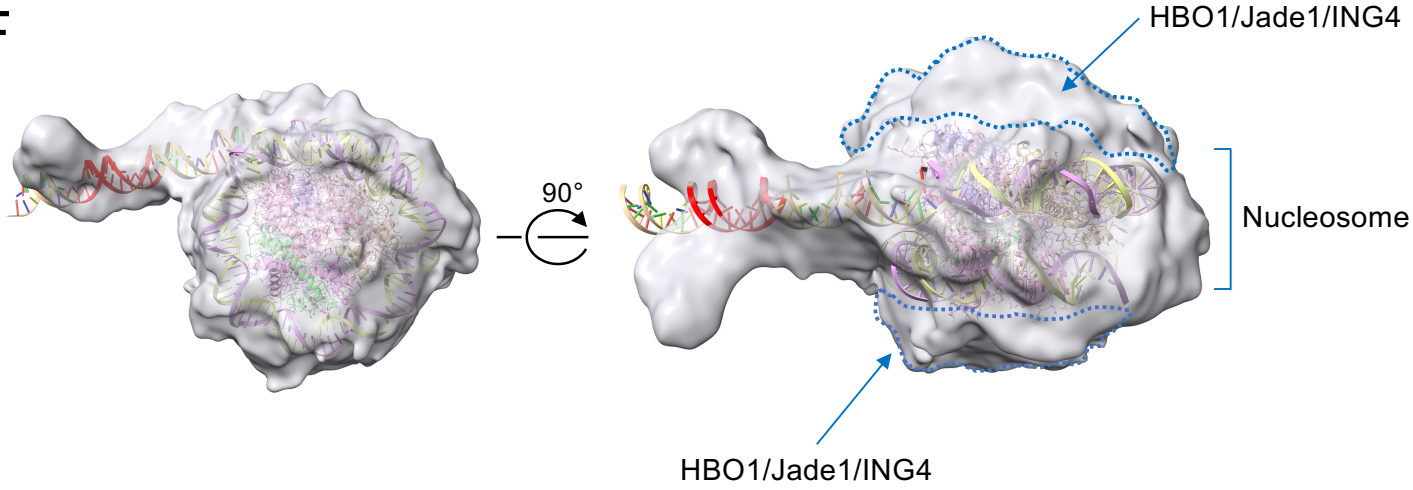
F